

**Nonconformally flat initial data for binary compact objects**Kōji Uryū,<sup>1</sup> François Limousin,<sup>2</sup> John L. Friedman,<sup>3</sup> Ericourgoulhon,<sup>2</sup> and Masaru Shibata<sup>4</sup><sup>1</sup>*Department of Physics, University of the Ryukyus, Senbaru, Nishihara, Okinawa 903-0213, Japan*<sup>2</sup>*Laboratoire Univers et Théories, UMR 8102 du CNRS, Observatoire de Paris, Université Paris Diderot, F-92190 Meudon, France*<sup>3</sup>*Department of Physics, University of Wisconsin-Milwaukee, P.O. Box 413, Milwaukee, Wisconsin 53201, USA*<sup>4</sup>*Yukawa Institute for Theoretical Physics, Kyoto University, Kyoto 606-8502, Japan*

(Received 6 August 2009; published 2 December 2009)

A new method is described for constructing initial data for a binary neutron-star system in quasiequilibrium circular orbit. Two formulations for nonconformally flat data, waveless and near-zone helically symmetric, are introduced; in each formulation, the Einstein-Euler system, written in  $3 + 1$  form on an asymptotically flat spacelike hypersurface, is exactly solved for all metric components, including the spatially nonconformally flat potentials, and for irrotational flow. A numerical method applicable to both formulations is explained with an emphasis on the imposition of a spatial gauge condition. Results are shown for solution sequences of irrotational binary neutron-stars with matter approximated by parameterized equations of state that use a few segments of polytropic equations of state. The binding energy and total angular momentum of solution sequences computed within the conformally flat—Isenberg-Wilson-Mathews—formulation are closer to those of the third post-Newtonian (3PN) two point particles up to the closest orbits, for the more compact stars, whereas sequences resulting from the waveless/near-zone helically symmetric formulations deviate from the 3PN curve even more for the sequences with larger compactness. We think it likely that this correction reflects an overestimation in the Isenberg-Wilson-Mathews formulation as well as in the 3PN formula, by  $\sim 1$  cycle in the gravitational-wave phase during the last several orbits. The work suggests that imposing spatial conformal flatness results in an underestimate of the quadrupole deformation of the components of binary neutron-star systems in the last few orbits prior to merger.

DOI: [10.1103/PhysRevD.80.124004](https://doi.org/10.1103/PhysRevD.80.124004)

PACS numbers: 04.25.D-, 04.25.dk, 04.25.Nx, 04.40.Dg

**I. INTRODUCTION**

Inspiral to merger of binary neutron stars (BNS) is one of the most promising sources of ground-based gravitational-wave detectors. A fully general relativistic numerical simulation is the unique approach to predict the gravitational waveform from the late inspiral to merger phase. Such a simulation begins with preparing quasiequilibrium initial data with a close orbital separation  $\sim 45$ – $50$  km.

Quasiequilibrium initial data for binary neutron stars introduce two kinds of inaccuracies into inspiral simulations. One is due to ignoring the radial component of the velocity of orbiting stars, the other to artificial restrictions on the geometry of the initial hypersurface [1]. A common choice for the geometry of the initial hypersurface is a conformally flat three-geometry [2,3], and a similarly restrictive alternative is presented in [4].<sup>1</sup> The former error is reduced by adding radial velocity to minimize the oscillation around the inspiral orbit, where the radial velocity may be determined empirically or calculated from the post-Newtonian formula of inspiraling point masses. Both errors become negligible if the initial separation of the binary is large enough, possibly five orbits or more before the

merger; but increasing separation increases the cost of computing time, and maintaining accuracy in numerical simulations may still be an issue.<sup>2</sup>

In a previous paper [7], we have reported that the inaccuracy of the binary orbit arising from spatial conformal flatness can be largely removed if one solves the full Einstein equation for all metric components, including the nonconformally flat part of the spatial metric, on a Cauchy surface  $\Sigma_t$ , using the formulation presented in [8–10]. In this formulation, Einstein's equation is written in a  $3 + 1$  form and the time derivative of the conformal three metric,  $\partial_t \tilde{\gamma}_{ab}$ , which carries the dynamics of the spacetime in our choice of the gauge, is set to zero.  $\tilde{\gamma}_{ab}$  is conformally related to the spatial metric  $\gamma_{ab}$  in each slice  $\Sigma_t$  by  $\gamma_{ab} = \psi^4 \tilde{\gamma}_{ab}$ , with  $\psi$  a conformal factor. As a result, the field equations for the metric components become elliptic equations on an initial slice  $\Sigma_t$ , and they yield an asymptotically flat metric. We call this approach the waveless (WL) formulation.

We have also experimented with another formulation for quasiequilibrium initial data in which all components of the metric are computed; preliminary results were presented in [11]. In this approach, helical symmetry is imposed in the near zone from the center of mass to the radius

<sup>1</sup>For the computation of black hole-neutron star binary in quasiequilibrium, see e.g. [5]

<sup>2</sup>For long-term simulation of binary black hole inspirals and matching to the post-Newtonian results, see e.g. [6]

$\sim \lambda = \pi/\Omega$ , and either the WL formulation is applied outside, or the computational domain is truncated at this radius. Here,  $\Omega$  is the orbital angular velocity and  $\lambda$  is the wavelength of the dominant, primarily  $\ell = m = 2$  quadrupole, mode of the gravitational waves expected to be radiated from the system. In this paper, we discuss the near-zone helically symmetric (NHS) formulation together with the WL formulation, for which numerical methods are common.

A significant difference in the binding energy and total angular momentum between the solutions from WL/NHS formulations and those from a conformally flat formulation, the Isenberg-Wilson-Mathews (IWM) formulation [12,13], is found and is discussed in the later section. In the IWM formulation, the solution sequences—the plots of these quantities as functions of orbital angular velocity—become closer to those of third post-Newtonian (3PN) point particles up to the closest orbits when the compactness of each star is increased. In contrast, sequences obtained from the WL/NHS formulations deviate more from the 3PN curve for larger compactness.

We expect waveless and helically symmetric solutions to accurately approximate the outgoing metric in the near zone, where the gravitational-wave amplitude is small compared to the Coulomb part of each metric potential. Results of Ref. [11] and of the present paper support this expectation by showing that corresponding WL and NHS solutions nearly coincide.

Several groups have developed simulation codes for BNS inspirals and merger; stable long-term simulations [14,15], magnetized BNS simulations [16], and black hole-neutron star binary merger simulations [17] are now feasible. As mentioned above, however, accurate modeling of the last several orbits of inspiraling binary compact object using quasiequilibrium sequences will be still useful, because the lower computational cost allows one to study gravitational-wave sources by exploring a wider parameter space, varying the mass ratio and the dense matter equation of state (EOS). One of the other applications will be the comparison with the results of simulations, which becomes a reliable calibration for both of the numerical solutions.

This paper is organized as follows: In Sec. II we describe the WL/NHS formulations. These are essentially identical to those introduced in our previous papers [9–11], except for a few modifications suitable for coding. All equations used in actual coding are written in Appendix A in detail. As a model for the EOS of high density matter, the parametrized EOS developed in [15,18] is used in the computations and is briefly introduced in this section. In Sec. III the numerical method is discussed, with emphasis on the major differences from the previous conformally flat code. In Sec. IV we report results from the WL/NHS computation of binary systems and of constant-rest-mass quasiequilibrium sequences.

In this paper, spacetime indices are Greek, spatial indices Latin, and the metric signature is  $- + + +$ . For

writing the basic equations, geometric units with  $G = c = 1$  are used, while for tabulating the numerical solutions, cgs units or other appropriate units are used.

## II. FORMULATION

### A. 3 + 1 decomposition and gauge conditions

The spacetime  $\mathcal{M} = \mathbb{R} \times \Sigma$  is foliated by a family of spacelike hypersurfaces  $(\Sigma_t)_{t \in \mathbb{R}}$  parametrized by  $t$ . The future-pointing unit normal  $n^\alpha$  to the hypersurface  $\Sigma_t$  is related to the generator  $t^\alpha$  of time translations, for which  $t^\alpha \nabla_\alpha t = 1$ , by

$$t^\alpha = \alpha n^\alpha + \beta^\alpha. \quad (1)$$

Here  $\alpha$  is the lapse function and  $\beta^\alpha$  the shift vector, with  $\beta^\alpha n_\alpha = 0$ .  $n^\alpha$  is related to the gradient of  $t$  by  $n_\alpha = -\alpha \nabla_\alpha t$ . It is also related to the helical vector  $k^\alpha$ , the generator of time translation in a rotating frame, by

$$k^\alpha = \alpha n^\alpha + \omega^\alpha, \quad (2)$$

where a spatial vector  $\omega^\alpha := \beta^\alpha + \Omega \phi^\alpha$  is the rotating shift in the rotating frame, and  $\Omega$  is a constant angular velocity of the rotating frame. The helical vector  $k^\alpha$  is not everywhere timelike, but it is transverse to the surface  $\Sigma_t$ , and normalized as  $k^\alpha \nabla_\alpha t = 1$ .

The spatial metric  $\gamma_{ab}(t)$  induced on  $\Sigma_t$  by the spacetime metric  $g_{\alpha\beta}$  is equal to the projection tensor orthogonal to  $n^\alpha$ ,  $\gamma_{\alpha\beta} = g_{\alpha\beta} + n_\alpha n_\beta$ , restricted to  $\Sigma_t$ . We introduce a conformal factor  $\psi$ , a conformally rescaled spatial metric  $\tilde{\gamma}_{ab}$ , and a flat spatial metric  $f_{ab}$ , with  $\gamma_{ab} = \psi^4 \tilde{\gamma}_{ab}$ , and with the conformal factor specified by the condition  $\tilde{\gamma} = f$ , where  $\tilde{\gamma}$  and  $f$  are the determinants of  $\tilde{\gamma}_{ab}$  and  $f_{ab}$ . In a chart  $(t, x^a)$ , the metric  $g_{\alpha\beta}$  has the form

$$ds^2 = -\alpha^2 dt^2 + \psi^4 \tilde{\gamma}_{ab} (dx^a + \beta^a dt)(dx^b + \beta^b dt). \quad (3)$$

Let us denote by  $h_{ab}$  and  $h^{ab}$  the differences between the conformal metric and the flat one:

$$\tilde{\gamma}_{ab} = f_{ab} + h_{ab}, \quad \tilde{\gamma}^{ab} = f^{ab} + h^{ab}. \quad (4)$$

The extrinsic curvature of each slice  $\Sigma_t$  is defined by

$$K_{ab} = -\frac{1}{2} \mathcal{L}_n \gamma_{ab}, \quad (5)$$

where the action of  $\mathcal{L}_n$  on  $\gamma_{ab}$  in the above definition, and on other spatial tensors hereafter, is given by

$$\mathcal{L}_n \gamma_{ab} := \frac{1}{\alpha} \partial_t \gamma_{ab} - \frac{1}{\alpha} \mathcal{L}_\beta \gamma_{ab}; \quad (6)$$

here  $\partial_t \gamma_{ab}$  is the pullback of  $\mathcal{L}_t \gamma_{\alpha\beta}$  to  $\Sigma_t$ , with  $\mathcal{L}_t$  the Lie derivative along the vector  $t^\alpha$  defined on  $\mathcal{M}$ , and  $\mathcal{L}_\beta$  is the Lie derivative along the spatial vector  $\beta^\alpha$  on  $\Sigma_t$ .

Einstein's equation is written in the 3 + 1 form

$$(G_{\alpha\beta} - 8\pi T_{\alpha\beta}) n^\alpha n^\beta = 0, \quad (7)$$

$$(G_{\alpha\beta} - 8\pi T_{\alpha\beta})\gamma_a^\alpha n^\beta = 0, \quad (8)$$

$$(G_{\alpha\beta} - 8\pi T_{\alpha\beta})\left(\gamma^{\alpha\beta} + \frac{1}{2}n^\alpha n^\beta\right) = 0, \quad (9)$$

$$(G_{\alpha\beta} - 8\pi T_{\alpha\beta})\left(\gamma_a^\alpha \gamma_b^\beta - \frac{1}{3}\gamma_{ab}\gamma^{\alpha\beta}\right) = 0. \quad (10)$$

These equations are the Hamiltonian and momentum constraints, the trace of the spatial projection combined with the Hamiltonian constraint, and the tracefree part of the spatial projection, respectively. They are solved for  $\psi$ ,  $\beta_a$ , the combination  $\alpha\psi$ , and  $h_{ab}$ . For perfect-fluid spacetimes, the stress-energy tensor  $T^{\alpha\beta}$  is written

$$T^{\alpha\beta} = (\epsilon + p)u^\alpha u^\beta + pg^{\alpha\beta}, \quad (11)$$

where  $\epsilon$  is the energy density,  $p$  the pressure, and  $u^\alpha$  the 4-velocity of the fluid.

The above set of equations are solved imposing as coordinate conditions the maximal slicing condition,

$$K = 0, \quad (12)$$

and the generalized Dirac gauge condition [9–11],

$$\overset{\circ}{D}_b \tilde{\gamma}^{ab} = \overset{\circ}{D}_b h^{ab} = 0, \quad (13)$$

where  $\overset{\circ}{D}_a$  is the covariant derivative associated with the flat metric  $f_{ab}$ . Concrete forms of Eqs. (7)–(10) are presented in Appendix A.

## B. Waveless and near-zone helically symmetric formulations

As a model for binary compact objects in general relativity, helically symmetric spacetimes have been introduced [19] and studied by several authors [20–27]. Helically symmetric binary solutions for point particles in a post-Minkowski framework [28] analogous to the electromagnetic two-body solution [29], and for several toy models have been calculated [11].

Helically symmetric spacetimes do not admit flat asymptotics. However, it is expected that, up to a certain truncation radius where the energy of radiation does not dominate the gravitational mass of the system, solutions have an approximate asymptotic region in which gravitational waves are propagating in a curved background. Such a solution, however, has not yet been calculated successfully in the regime of strong gravity.

Helical symmetry,

$$\mathfrak{L}_k g_{\alpha\beta} = 0, \quad (14)$$

implies for the 3-metric and extrinsic curvature on a initial hypersurface  $\Sigma_t$ ,

$$\mathfrak{L}_k \gamma_{ab} = 0, \quad \mathfrak{L}_k K_{ab} = 0. \quad (15)$$

Using the relation  $k^\alpha = \alpha n^\alpha + \omega^\alpha$ , we have

$$\mathfrak{L}_n \gamma_{ab} = -\frac{1}{\alpha} \mathfrak{L}_\omega \gamma_{ab}, \quad (16)$$

$$\mathfrak{L}_n K_{ab} = -\frac{1}{\alpha} \mathfrak{L}_\omega K_{ab}. \quad (17)$$

Because  $k^\alpha$  is timelike in the fluid, helical symmetry for the fluid variables,

$$\mathfrak{L}_k u^\alpha = 0, \quad \mathfrak{L}_k \epsilon = 0, \quad \mathfrak{L}_k p = 0, \quad (18)$$

has the meaning of stationarity for a rotating observer.

Our formulation for the nonconformally flat data of binary compact objects in a quasicircular orbit is based on the helically symmetric formulation. We further impose either a waveless condition or near-zone helical symmetry in the gauge (12) and (13).

*a. Waveless formulation* As discussed in [10], the condition,  $\partial_t \tilde{\gamma}^{ab} = O(r^{-3})$ , is sufficient to enforce Coulomb-type fall-off in the asymptotics. For our waveless formulation in this paper, we impose the stronger condition

$$\partial_t \tilde{\gamma}_{ab} = 0, \quad (19)$$

which amounts to writing the extrinsic curvature as

$$\begin{aligned} K_{ab} &= \frac{1}{2\alpha} \mathfrak{L}_\beta \gamma_{ab} - \frac{1}{2\alpha} \gamma_{ab} \left(\frac{\tilde{\gamma}}{\gamma}\right)^{1/3} \partial_t \left(\frac{\gamma}{\tilde{\gamma}}\right)^{1/3} \\ &= \frac{1}{2\alpha} \mathfrak{L}_\beta \gamma_{ab} + \frac{1}{2\alpha} \gamma_{ab} \Omega \mathfrak{L}_\phi \ln \psi^4, \end{aligned} \quad (20)$$

where helical symmetry is used to get the second equality. Only the first term on the right-hand side (r.h.s.) remains in the maximal slicing condition. Because the trace of Eq. (20) has the same form for  $K = 0$  as the trace of the original Eq. (5), the waveless condition (19) does not affect the maximal slicing condition. Note that the second term of the r.h.s. of Eq. (20) does not appear in the tracefree part of  $K_{ab}$ ; in other words, the time derivative of the conformal factor  $\psi$  does not appear in the initial value formulation in this slicing. The other time derivatives are given by the helical symmetry conditions, Eqs. (17) and (18).

*b. Near-zone helically symmetric formulation* Near-zone helical symmetry means that we impose helically symmetric conditions (16)–(18) in the region from the center of the source to about one wavelength of the  $\ell = m = 2$  mode of the gravity wave,  $r \lesssim \lambda := \pi/\Omega$ ; we then either truncate the domain of numerical computation at this radius or use the waveless formulation outside. The latter implies for  $K_{ab}$  the condition

$$K_{ab} = \begin{cases} \frac{1}{2\alpha} \mathfrak{L}_\omega \gamma_{ab} & \text{for } r < a\lambda, \\ \frac{1}{2\alpha} \mathfrak{L}_\beta \gamma_{ab} + \frac{1}{2\alpha} \gamma_{ab} \Omega \mathfrak{L}_\phi \ln \psi^4 & \text{for } r \geq a\lambda, \end{cases} \quad (21)$$

where the constant  $a$ , the coordinate radius of the helically symmetric zone in units of  $\lambda = \pi/\Omega$ , is restricted to

$a \lesssim 1.5$ . Without this restriction, iterations fail to converge to a binary solution. In the near-zone-helical + outside-waveless formulation, all metric components, including those of the spatial metric, have Coulomb-type fall-off. We have compared the NHS solution to the WL solution in our previous paper [11] and confirmed that the difference in the nonconformal flat part of the spatial metric is about 1% for the BNS of  $M_1/R \sim 0.17$ , where  $M_1/R$  is the compactness, the ratio of the gravitational mass to the circumferential radius of a spherical star having the same rest mass as each component star of the binary.

### C. Formulation for the irrotational flow

The late stage of BNS inspiral is modeled by a constant-rest-mass sequence of quasiequilibrium solutions with negligible spins and magnetic fields, a description appropriate to a binary of old pulsars with spin periods longer than 100 ms. Since the viscosity of the high density matter is expected to be negligible, a neutron star in a binary system is not spun up by the tidal torque during the inspirals. Hence, the flow field remains approximately irrotational, and each neutron star is modeled by an irrotational perfect fluid [30].

The equation of motion,  $\nabla_\beta T_\alpha^\beta = 0$ , for a perfect fluid has the form

$$\begin{aligned} \nabla_\beta T_\alpha^\beta &= \rho[u^\beta \nabla_\beta(hu_\alpha) + \nabla_\alpha h] + hu_\alpha \nabla_\beta(\rho u^\beta) \\ &\quad - \rho T \nabla_\alpha s = 0, \end{aligned} \quad (22)$$

where  $s$  is the entropy per baryon mass,  $h$  is the relativistic enthalpy per baryon mass  $h := (\epsilon + p)/\rho$ , and local thermodynamic equilibrium  $dh = Tds + dp/\rho$  is assumed. We assume constant entropy per baryon ( $s = \text{const}$ ) everywhere inside the neutron star, together with a one-parameter EOS,

$$p = p(\rho). \quad (23)$$

The form

$$u^\beta \nabla_\beta(hu_\alpha) + \nabla_\alpha h = 0 \quad (24)$$

of the relativistic Euler equation then follows from local conservation of baryon mass,

$$\nabla_\alpha(\rho u^\alpha) = 0. \quad (25)$$

Written in terms of the Lie derivative along  $u^\alpha$ , these last equations have the form

$$\frac{1}{\sqrt{-g}} \mathfrak{L}_u(\rho \sqrt{-g}) = 0, \quad (26)$$

$$\mathfrak{L}_u(hu_\alpha) + \nabla_\alpha h = 0. \quad (27)$$

A state is stationary state in the rotating frame if it is helically symmetric, if each physical field is Lie derived by the helical vector field  $k^\alpha$ , as in Eq. (18), or

$$\mathfrak{L}_k(\rho u^t \sqrt{-g}) = 0, \quad \text{and} \quad \mathfrak{L}_k(hu_\alpha) = 0, \quad (28)$$

where  $u^t$  is the scalar  $u^\alpha \nabla_\alpha t$ .

The relativistic Euler Eq. (24) can be rewritten as

$$u^\beta \omega_{\beta\alpha} = 0, \quad (29)$$

where

$$\omega_{\beta\alpha} := \nabla_\beta(hu_\alpha) - \nabla_\alpha(hu_\beta) \quad (30)$$

is the relativistic vorticity tensor. This implies that, for irrotational flow,  $hu_\alpha$  has a potential  $\Phi$ ,

$$hu_\alpha = \nabla_\alpha \Phi, \quad (31)$$

and hence the relativistic Euler equation has a first integral. With a spatial velocity  $v^\alpha$  in the rotating frame defined by

$$u^\alpha = u^t(k^\alpha + v^\alpha), \quad (32)$$

where  $v^\alpha n_\alpha = 0$ , Eq. (27) becomes

$$\begin{aligned} \mathfrak{L}_u(hu_\alpha) + \nabla_\alpha h &= u^t \left[ \mathfrak{L}_{k+v}(hu_\alpha) + \nabla_\alpha \frac{h}{u^t} \right] \\ &= u^t \nabla_\alpha \left( \mathfrak{L}_v \Phi + \frac{h}{u^t} \right) = 0; \end{aligned} \quad (33)$$

therefore the first integral is

$$\mathfrak{L}_v \Phi + \frac{h}{u^t} = \mathcal{E}, \quad (34)$$

where  $\mathcal{E}$  is a constant.<sup>3</sup> Note that Eqs. (28) and (31) imply a flow with  $\mathfrak{L}_k \Phi = \text{constant}$ . Such a flow is both irrotational and helically symmetric with the shape of the star fixed in the rotating frame. Solutions describing irrotational binaries in Newtonian and post-Newtonian gravity are found in [31], and details of the formulation for helically symmetric irrotational flow are given in [20,32].

There are three fluid variables and two parameters to be determined in the above formulation. The fluid variables are a thermodynamic variable, the velocity potential  $\Phi$ , and the time component of the 4-velocity  $u^t$ ; and these are calculated from the first integral (34), the rest-mass conservation Eq. (26), and the normalization of the 4-velocity,  $u_\alpha u^\alpha = -1$ . A concrete form of these equations are presented in Appendix A 3. For the independent thermodynamic variable, we choose  $q := p/\rho$ , and other thermodynamic variables are determined from the thermodynamic relations and the one-parameter EOS, which are briefly explained in the next section. The number of fluid variables and parameters are augmented in the numerical computation, which is mentioned in Appendix B 2 (or see [33]).

<sup>3</sup>Cartan identity  $k^\beta \omega_{\beta\alpha} = \mathfrak{L}_k(hu_\alpha) - \nabla_\alpha(hu_\beta k^\beta)$  implies, for the helically symmetric irrotational flow satisfying  $\mathfrak{L}_k(hu_\alpha) = 0$  and  $\omega_{\beta\alpha} = 0$ , a relation,  $hu_\alpha k^\alpha = \text{constant}$ , equivalent to Eq. (34).

### D. Parametrized equations of state

Recently, a parametrization for the EOS of nuclear matter has been studied, and it is shown that a parametrized EOS with three polytropic intervals approximates with fair accuracy a variety of current candidate EOS, over a range of densities that extends from the inner crust to the maximum neutron-star density [18]. Two of these intervals and three parameters cover densities below the central density of a  $1.4M_\odot$  neutron star, and waveforms from binary inspiral can be used to constrain this three-dimensional subspace of the parameter space [15]. This parametrized EOS is used in our models for BNS data.

#### 1. Construction of piecewise polytropic EOS

In presenting these piecewise polytropes, it is helpful to introduce a relativistic Emden function  $q$  by

$$q := p/\rho \quad (35)$$

and to write the remaining thermodynamic variables in terms of  $q$ . For an isentropic flow with  $s = 0$ , the local first law of thermodynamic equilibrium,  $dh = Tds + \frac{1}{\rho} dp$ , takes the form

$$dh = \frac{1}{\rho} dp, \quad (36)$$

where  $h$  is the enthalpy per baryon mass.

A piecewise polytropic EOS is given by

$$p = K_i \rho^{\Gamma_i}, \quad (37)$$

in the intervals  $\rho \in [\rho_{i-1}, \rho_i)$ ,  $i = 1, \dots, N$ , with  $\rho_0 = 0$  and  $\rho_N = \infty$ . In this section the subscript  $i$  denotes the  $i$ th interval, associated with a set of constants  $\{\Gamma_i, K_i\}$  with  $i = 1, \dots, N$ , and labels the value of quantities at the higher density side of each interval,  $[\rho_{i-1}, \rho_i)$ . Because we consider only continuous EOS,  $p_i, h_i, \epsilon_i$  and  $q_i$  are the values of each of these quantities at density  $\rho_i$ .

The constant indices  $\Gamma_i$  are  $N$  model parameters, and values of one thermodynamic variable at interfaces comprise a set of  $N - 1$  model parameters. A requirement that the pressure at the interface is continuous,

$$K_i \rho_i^{\Gamma_i} = K_{i+1} \rho_i^{\Gamma_{i+1}}, \quad (38)$$

uniquely specifies values of  $K_i$  up to one free parameter, one of  $K_i$  of a specific  $i$ th interval, which is usually specified by prescribing the value of pressure  $p_i$  at the corresponding interface density  $\rho_i$ . Therefore we have  $2N$  parameters for a parametrized EOS with  $N$  intervals.

To compute other thermodynamic quantities from  $q$ , we use the following relations, valid in the  $i$ th interval,  $q \in [q_{i-1}, q_i)$ :

$$\rho = K_i^{-1/(\Gamma_i-1)} q^{1/(\Gamma_i-1)}, \quad (39)$$

$$p = K_i^{-1/(\Gamma_i-1)} q^{\Gamma_i/(\Gamma_i-1)}, \quad (40)$$

$$h - h_{i-1} = \frac{\Gamma_i}{\Gamma_i - 1} (q - q_{i-1}), \quad (41)$$

$$\epsilon = \rho h - p, \quad (42)$$

where Eq. (41) is obtained by integrating the relation

$$dh = \frac{1}{\rho} dp = \frac{\Gamma_i}{\Gamma_i - 1} dq \quad (43)$$

in the  $i$ th interval  $q \in [q_{i-1}, q_i)$ . Here,

$$h_i = h_0 + \sum_{j=1}^i \frac{\Gamma_j}{\Gamma_j - 1} (q_j - q_{j-1}), \quad (44)$$

with  $h_0 = 1$  and  $q_0 = 0$ .

#### 2. Choice for the parameters

In the latter sections, we present the results of quasi-equilibrium BNS solutions calculated using two types of parametrized EOS. The first EOS contains one free parameter, which is used to estimate the accuracy of the measurement of the EOS parameter, and the neutron-star radius, by gravitational-wave observations of the inspirals of BNS [15]. The second EOS is a four-parameter fit to the candidates of neutron-star EOS. Those candidate EOS are tabulated nuclear EOS, and the parametrized EOS with four parameters approximates each candidate within the rms residual typically in the order of  $\sim 0.1\%$ , and  $\sim 4.3\%$  for the worst case [18].

The parametrized EOS with one parameter uses two polytropic intervals. The lower density interval approximates the known subnuclear density EOS, the fixed crust EOS, around  $0.1\rho_{\text{nuc}} \sim \rho_{\text{nuc}}$  by setting  $(\Gamma_0, K_0) = (1.35692, 3.59389 \times 10^{13})$ . Here,  $\rho_{\text{nuc}}$  is the nuclear saturation density, and the constant  $K_0$  is in cgs units which give the pressure  $p$  in dyn/cm<sup>2</sup>. For the second polytropic interval at the higher density side, the adiabatic index is set  $\Gamma_1 = 3$ . Then, the pressure  $p_1$  at the density  $\rho_1 = 10^{14.7}$  g/cm<sup>3</sup> is chosen as a parameter, and the dividing density at the fixed crust and the next polytropic piece  $\rho_0$  is determined as the intersection of the two intervals. Further details are found in [15].

The four-parameter fit uses the same crust EOS as above, and three other polytropic intervals. The adiabatic indices of higher polytropic intervals  $\{\Gamma_1, \Gamma_2, \Gamma_3\}$ , and the pressure  $p_1$  at the interface between  $i = 1$  and 2 are chosen as fitting parameters, while the dividing density  $\rho_0$  is evaluated in the same way as above, and other dividing densities are fixed as  $\rho_1 = 10^{14.7}$  g/cm<sup>3</sup> and  $\rho_2 = 10^{15}$  g/cm<sup>3</sup>. The EOS parameters and corresponding data for the spherical solutions are summarized in the later Sec. IV. Further details for the four-parameter fit are found in [18].

### III. COMPUTATION

A system of elliptic equations and algebraic relations are solved applying a self-consistent field iteration scheme [34]. Recently, the convergence of such scheme for Newtonian barotropic stars has been mathematically analyzed in [35].

The WL/NHS code for the irrotational BNS presented in this paper is developed on top of the former BNS code in which the IWM formulation is used [36]. Another version of the WL/NHS code, based on the triaxially deformed rotating neutron-star code described in [33], has been developed, and its results are presented elsewhere. The numerical method used in these codes is briefly repeated in Appendix B.

#### A. Imposition of Dirac gauge

The primary difference between the WL/NHS code and an IWM code is the computation of the nonconformally flat part of the spatial metric  $\tilde{\gamma}_{ab} = f_{ab} + h_{ab}$ . The conformal spatial metric  $\tilde{\gamma}_{ab}$  has to satisfy two conditions,  $\tilde{\gamma} = f$  and  $\overset{\circ}{D}_b \tilde{\gamma}^{ab} = 0$ , which turn out not to be automatically satisfied when the spatial tracefree part of Einstein's equation (10) or its concrete form in the code, either Eq. (A57) or (A60), is solved for  $h_{ab}$ . To impose these conditions on  $\tilde{\gamma}_{ab}$  accurately, we first make a gauge transformation of  $h_{ab}$  to satisfy  $\overset{\circ}{D}_b h^{ab} = 0$ , and we then correct the conformal factor to enforce the relation  $\gamma = \psi^{12} f$  at each iteration cycle. Note that these two conditions are not explicitly imposed in Eq. (A57) or (A60), and they are violated mainly due to the numerical error of finite differencing.

The gauge vector is calculated numerically by the following procedure: a perturbation of the spatial metric  $\delta\gamma_{ab}$

$$\delta\gamma_{ab} \rightarrow \delta\gamma_{ab} - \overset{\circ}{D}_a \xi_b - \overset{\circ}{D}_b \xi_a, \quad (45)$$

implies, to the same order, that the conformally rescaled metric with  $\tilde{\gamma} = f$  satisfies

$$\delta\tilde{\gamma}_{ab} \rightarrow \delta\tilde{\gamma}_{ab} - \overset{\circ}{D}_a \xi_b - \overset{\circ}{D}_b \xi_a + \frac{2}{3} f_{ab} \overset{\circ}{D}_c \xi^c. \quad (46)$$

We adjust  $h_{ab}$  to this order to satisfy the Dirac gauge condition; namely, writing

$$h'_{ab} = h_{ab} - \overset{\circ}{D}_a \xi_b - \overset{\circ}{D}_b \xi_a + \frac{2}{3} f_{ab} \overset{\circ}{D}_c \xi^c, \quad (47)$$

we let  $h'_{ab}$  satisfy the Dirac gauge condition to linear order in  $h_{ab}$ ,  $\overset{\circ}{D}^b h'_{ab} = 0$ , which leads to

$$\overset{\circ}{\Delta} \xi_a + \frac{1}{3} \overset{\circ}{D}_a \overset{\circ}{D}^b \xi_b = \overset{\circ}{D}^b h_{ab}. \quad (48)$$

This equation is solved by introducing the decomposition

$$\xi_a = G_a - \frac{1}{4} \overset{\circ}{D}_a B, \quad (49)$$

which results in a set of elliptic equations,

$$\overset{\circ}{\Delta} G_a = \overset{\circ}{D}^b h_{ab}, \quad \text{and} \quad \overset{\circ}{\Delta} B = \overset{\circ}{D}^a G_a. \quad (50)$$

These equations (50) are solved using the same Poisson solver described in Appendix B, and a solution is substituted in Eq. (49) and then in Eq. (47). In the r.h.s. of Eq. (47),  $h_{ab}$  is calculated from the tracefree part of Einstein's equation, either Eq. (A57) or (A60), and it is replaced by  $h'_{ab}$ , which satisfies the Dirac gauge condition more accurately. We have also experimented with a transformation of the contravariant components of  $h^{ab}$  analogous to Eq. (47), and let  $\overset{\circ}{D}_b h^{ab} = 0$  be satisfied; however, the results did not change.

After the above gauge transformation, the condition  $\tilde{\gamma} = f$  is imposed by adjusting the conformal factor  $\psi$  to

$$\psi' = \psi \left( \frac{\tilde{\gamma}'}{f} \right)^{1/12}, \quad (51)$$

where  $\tilde{\gamma}'$  is the determinant of  $\tilde{\gamma}'_{ab} = f_{ab} + h'_{ab}$ . Note that, to impose  $\tilde{\gamma} = f$ , we do not change the value of  $h'_{ab}$ . These two corrections to  $h_{ab}$  and  $\psi$  are made once per iteration.

The other parts of the method of computation, including the iteration scheme, are common to our previous codes [33,36,37], which are briefly reviewed in Appendix B.

#### B. Coordinate and grid parameters

The WL/NHS code uses two coordinate patches: a spherical patch, called the central coordinate system, on which the metric components are calculated, and a surface-fitted spherical-coordinate patch on which the fluid variables are computed. The origin of the central coordinates  $(r, \theta, \phi)$  is the mass center of the binary system, and that of the surface-fitted coordinates  $(\hat{r}_f, \theta_f, \phi_f)$  is the geometric center of the component star, where  $\hat{r}_f$  is related to the radial coordinate  $r_f$  by  $\hat{r}_f = r_f/R(\theta_f, \phi_f)$  and  $R(\theta_f, \phi_f)$  is the surface of the star. We match the radial coordinate lines at  $(\theta, \phi) = (\pi/2, 0)$  of the central coordinates, and that of the surface-fitted coordinates  $(\theta_f, \phi_f) = (\pi/2, 0)$ , and set the  $\theta = 0$  and  $\theta_f = 0$  lines to be parallel. Only the octant of the whole space for the central coordinate is solved,

TABLE I. Summary of grid parameters. (CC) stands for the central coordinates, and (SFC) for the surface-fitted coordinates.

$N_r$ :	Number of intervals $\Delta r_i$ in $r \in [0, r_b]$ (CC).
$n_r$ :	Number of intervals $\Delta r_i$ in $r \in [0, r_c]$ (CC).
$N_\theta$ :	Number of intervals $\Delta \theta_i$ in $\theta \in [0, \pi/2]$ (CC).
$N_\phi$ :	Number of intervals $\Delta \phi_i$ in $\phi \in [0, \pi/2]$ (CC).
$N_{\hat{r}_f}$ :	Number of intervals $\Delta \hat{r}_i$ in $\hat{r}_f \in [0, 1]$ (SFC).
$N_{\theta_f}^i$ :	Number of intervals $\Delta \theta_i$ in $\theta_f \in [0, \pi/2]$ (SFC).
$N_{\phi_f}^i$ :	Number of intervals $\Delta \phi_i$ in $\phi_f \in [0, \pi]$ (SFC).

TABLE II. Coordinate parameters, and the number of grid points used in this paper.  $R_0$  is the geometrical radius of the neutron star along the  $(\theta_f, \phi_f) = (\pi/2, 0)$  line.  $l_{\max}$  and  $l_{\max}^f$  are the highest multipoles included in the Legendre expansion in the central and surface-fitted coordinates, respectively.

$r_b$	$r_c$	$N_r$	$n_r$	$N_\theta$	$N_\phi$	$l_{\max}$	$N_r^f$	$N_\theta^f$	$N_\phi^f$	$l_{\max}^f$
$10^4 R_0$	$5R_0$	250	160	64	64	40	32	32	24	8

while a quarter for the surface-fitted coordinate. The spherical coordinates correspond to the Cartesian coordinates in the usual way; the  $(\theta, \phi) = (\pi/2, 0)$  line to the (positive)  $x$  axis, the  $(\pi/2, \pi/2)$  line to the  $y$  axis, and the  $\theta = 0$  line to the  $z$  axis.

The accuracy of the numerical solutions depends on the resolution of the finite differencing determined by the grid spacings  $(\Delta r, \Delta\theta, \Delta\phi)$ , and the order of the truncation of multipole expansion  $\ell_{\max}$ . The latter is constrained by the resolution since the multipoles involved in the Green's function, which oscillates rapidly for the larger  $\ell$ , should be resolved on the grids. The radial grid spacing  $\Delta r$  of the central coordinates is equidistant for  $r \in [0, r_c]$ , and increases in geometric progression for  $r \in [r_c, r_b]$ . The grid spacings of the other coordinates are equidistant. For further details, see [33,36,37]. For the grid parameters defined in Table I, we choose values listed in Table II. Typically, 1 cycle of iteration takes about 70 s for this grid setup using a single core of Intel Xeon CPU X5450 with 3.00 GHz clock.

## IV. QUASIEQUILIBRIUM SOLUTIONS

### A. Behavior of $h_{ij}$ for selected solutions

Quasiequilibrium solutions of irrotational BNS are calculated for the various sets of EOS parameters summarized in Table III. As an example of the WL solutions, we present in Fig. 1 contours of selected components of  $h_{ij}$  for the parametrized EOS HB, with orbital radius  $d/R_0 = 1.5$ ,

where  $R_0$  is the coordinate radius (half the diameter) of the neutron star along the  $x$  axis. For a qualitative comparison, contours are also shown for the leading order terms  $O(r^{-1})$  of the asymptotic solution of  $h_{ij}$  in a second order post-Newtonian (2PN) approximation with maximal slicing and a transverse-traceless gauge for  $h_{ij}$ , as derived in [38] [see, Eq. (5.30)], namely,

$$h_{ij} = \frac{1}{r} \left\{ \frac{1}{4} I_{ij} + \frac{3}{4} n^k (n^i I_{kj} + n^j I_{ki}) - \frac{5}{8} n^i n^j I_{kk} + \frac{3}{8} n^i n^j n^k n^l I_{kl} + \frac{1}{8} \delta_{ij} I_{kk} - \frac{5}{8} \delta_{ij} n^k n^l I_{kl} \right\} + O(r^{-2}), \quad (52)$$

where

$$I_{ij} = \int \rho x^i x^j d^3x, \quad \text{and} \quad n^i = \frac{x^i}{r}. \quad (53)$$

In the quadrupole integrals  $I_{ij}$ , we substituted two  $1.35M_\odot$  point masses, separated by the same coordinate length as the above WL solution. The region shown in these figures does not extend far enough to have asymptotic behavior, though the contours qualitatively agree.

In Fig. 2, selected components of  $h_{ij}$  are plotted along the  $x$  axis for the cases with parametrized EOS 2H, HB, and 2B, from top to the bottom panels. In each case the orbital radius is again  $d/R_0 = 1.5$ . In our models, the gravitational mass of the corresponding spherical star is  $M_1 = 1.35M_\odot$  and  $M_1/R$  of each EOS increases in the order of 2H, HB, 2B (see Table III), which is reflected by the increasing amplitude of  $h_{ij}$ . Here and after, the *compactness* of each component star in the binary system means the value of  $M_1/R$  for a single spherical star with the same rest mass.

In the right panels, corresponding to the left panels, log-log plots of the  $h_{yy}$  and  $h_{zz}$  components are shown up to the

TABLE III. Parameters of each EOS and properties of the spherical neutron-star model based on that EOS and having gravitational mass  $M_1 = 1.35M_\odot$ . The pressure  $p_1$  [dyn/cm<sup>2</sup>] is the value at the dividing density  $\rho_1 = 10^{14.7}$  g/cm<sup>3</sup>, and values of  $\log(p_1)$  and  $\{\Gamma_1, \Gamma_2, \Gamma_3\}$  are taken from Table I of [15] and Table III of [18]. The parameters to fit the crust EOS are chosen as  $(\Gamma_0, K_0) = (1.35692, 3.59389 \times 10^{13})$  where  $K_0$  is in cgs units, and the dividing density  $\rho_0$  used to model the transition from the crust to the nuclear matter is tabulated in the log of  $\rho_0$  [g/cm<sup>3</sup>]. In the following calculations for BNS, a spherical solution of each EOS with gravitational mass  $M_1 = 1.35M_\odot$  is used as a reference, whose rest mass  $M_0$  in solar mass units, circumferential radius  $R$  in km, compactness  $M_1/R$  in the geometric unit  $G = c = 1$ , and log of the central density  $\rho_c$  in g/cm<sup>3</sup> are tabulated.

Model	$\log(\rho_0)$	$\log(p_1)$	$\Gamma_1$	$\Gamma_2$	$\Gamma_3$	$M_1[M_\odot]$	$M_0[M_\odot]$	$R$ [km]	$M_1/R$	$\log(\rho_c)$
2H	13.847	34.90	3	3	3	1.35	1.4549	15.224	0.13097	14.573
HB	14.151	34.40	3	3	3	1.35	1.4927	11.606	0.17181	14.918
2B	14.334	34.10	3	3	3	1.35	1.5251	9.7268	0.20500	15.141
SLy	14.165	34.384	3.005	2.988	2.851	1.35	1.4947	11.469	0.17385	14.934
APR1	14.294	33.943	2.442	3.256	2.908	1.35	1.5388	9.1385	0.21819	15.221
FPS	14.220	34.283	2.985	2.863	2.600	1.35	1.5055	10.702	0.18631	15.038
BGN1H1	14.110	34.623	3.258	1.472	2.464	1.35	1.4789	12.626	0.15792	14.912
ALF3	14.188	34.283	2.883	2.653	1.952	1.35	1.5069	10.350	0.19264	15.150

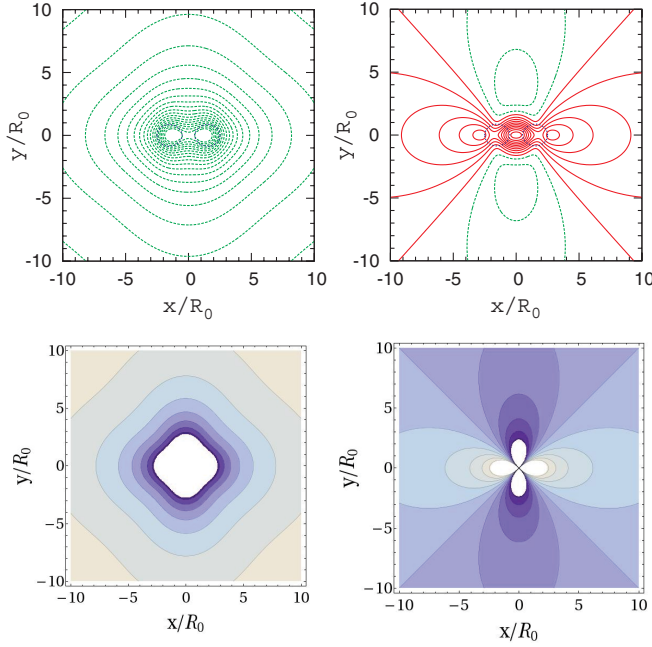


FIG. 1 (color online). Contours of  $(h_{xx} - h_{yy})/2$  (left panels) and  $h_{zz}$  (right panels) in the  $xy$  plane. Top panels are those of a WL solution with the EOS parameter HB and the orbital radius  $d/R_0 = 1.5$ , where  $R_0$  is the coordinate radius (a half of the diameter) of the neutron star along the  $x$  axis. Contours are drawn every 0.001 step, where the solid (dashed) contours in the top panels corresponds to positive (negative) values of  $h_{ij}$ . Thick dotted circles are the surface of neutron stars. Bottom panels are the contours of the 2PN asymptotic formula (52) calculated for the two point masses assuming the same coordinate separation  $d/R_0 = 1.5$ , and mass  $M = 1.35M_\odot \times 2$ . Contours are also drawn every 0.001 step. In the left top and bottom panels, the outermost contour (interrupted by the boundary of the figure) corresponds to  $-0.002$ . In the bottom two panels, contours out of range ( $< -0.01$  for the left panel, and  $\geq \pm 0.005$  for the right) are truncated.

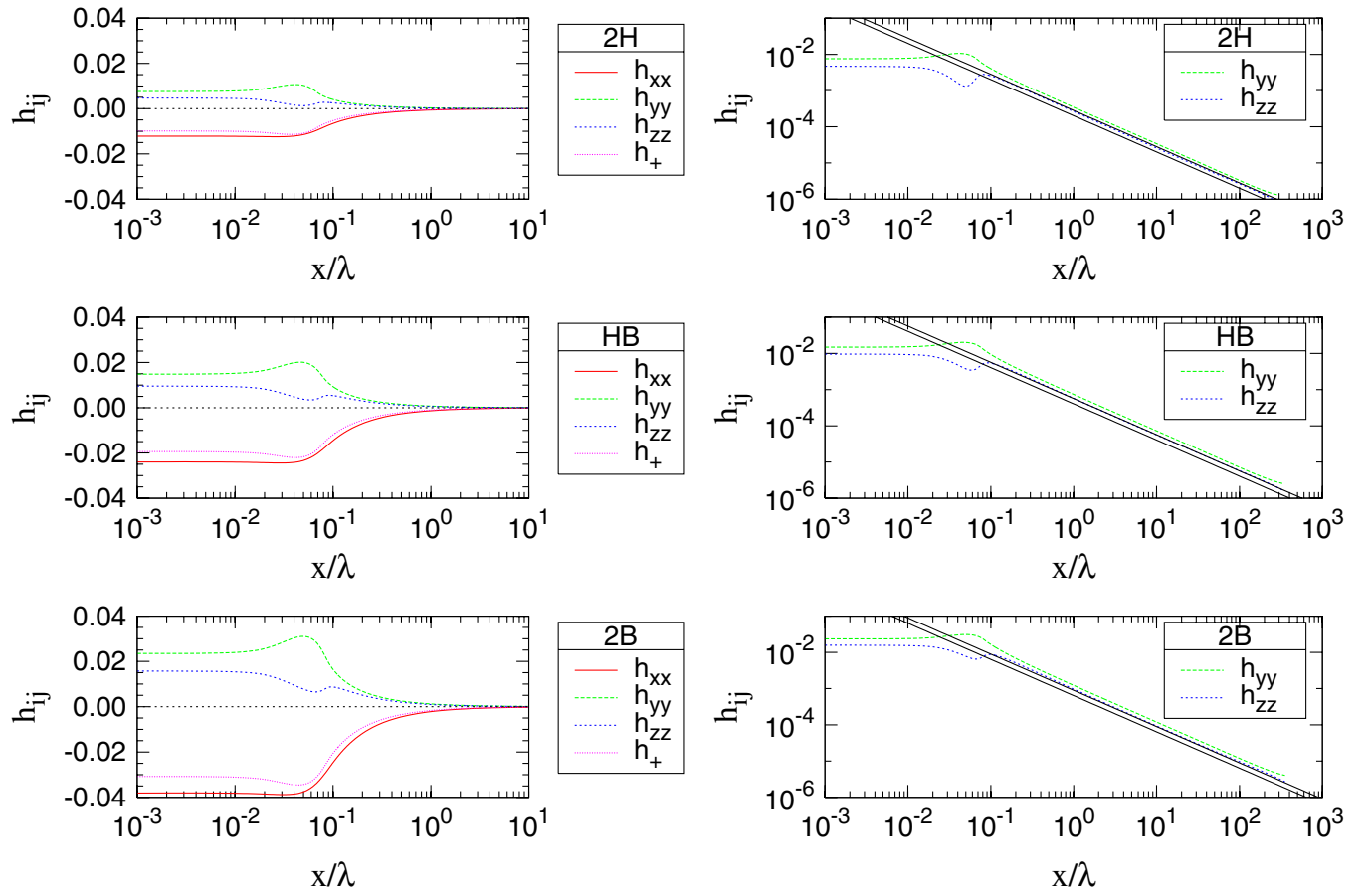


FIG. 2 (color online). Selected components of  $h_{ij}$  along the  $x$  axis of the WL solutions with the orbital radius  $d/R_0 = 1.5$  for parametrized EOS 2H, HB, and 2B, from top to bottom panels of both sides, respectively. Left (right) panels are log-linear (log-log) plots, where the  $x$  axis is normalized by  $\lambda := \pi/\Omega$ . Upper and lower thin solid lines in the right panels are, respectively, the  $h_{yy}$  and  $h_{zz}$  components of the asymptotic solutions (52) of two point mass,  $M_1 = 1.35M_\odot$  each, separated as the numerical solutions,  $d/R_0 = 1.5$ .  $h_+$  in left panels is defined by  $h_+ := (h_{xx} - h_{yy})/2$ .

boundary of the computational domain. Upper and lower thin black lines in the right panels are, respectively, the  $h_{yy}$  and  $h_{zz}$  components of the asymptotic solutions (52) of two point masses. These lines do not exactly match the  $h_{ij}$  contours of the corresponding numerical solutions for several reasons, including finite-size and higher order post-Newtonian effects. However, the lines shift systematically from the numerical  $h_{ij}$ , which suggest that the numerical  $h_{ij}$  scales properly in the asymptotic region (as well as in the near zone) as the compactness increases.

### B. Quasiequilibrium sequences with different compactness

A constant-rest-mass sequence of quasiequilibrium solutions for irrotational BNS is considered as a model for the last several orbits of inspiral before merger. Such sequences are computed for the models with different EOS parameters listed in Table III. The fixed rest mass of each model is that of a spherical star whose gravitational mass is  $M_1 = 1.35M_\odot$ . Quantities of the spherical star for each model are also presented in the same Table.

In Fig. 3, the binding energy  $E_b := M_{\text{ADM}} - M$  and the total angular momentum  $J$ , normalized by twice the gravitational mass of the spherical star  $M = 2M_1$ , are plotted for models 2H, HB, and 2B. In the top and middle panels, the results of the WL sequences are compared with the results of IWM sequences and of nonspinning point particles in 3PN circular orbits. Clearly, the IWM sequences coincide with the 3PN curve up to smaller separation (larger  $\Omega M$ ), whereas the WL sequences significantly deviate from the 3PN sequence. As the compactness (in this case from 2H to 2B) increases, the curves of the IWM sequence around the smallest separation come closer to the 3PN curve. In contrast to this, deviations of the WL sequences from the 3PN curve are even larger for the larger compactness.

In the bottom panel of the Fig. 3, the binding energy  $E_b := M_{\text{ADM}} - M$  of the WL sequences are compared with the results of the NHS sequences. Clearly, the difference in the binding energy of two formulations is less than a percent; that is, the WL solutions almost coincide with the helically symmetric solution in the near zone.

In [10], we have derived asymptotic conditions for equality  $M_{\text{ADM}} = M_{\text{K}}$  of the ADM and Komar masses [39], which is related to the relativistic virial relation for the equilibrium [40],

$$\int x^a \gamma_a^\alpha \nabla_\beta T_\alpha^\beta \sqrt{-g} d^3x = 0. \quad (54)$$

In the WL/NHS formulation, the asymptotic fall-off of each field is sufficiently fast to enforce the equality. In Fig. 4, we evaluate the values of the fractional differences  $|M_{\text{ADM}} - M_{\text{K}}|/M_{\text{ADM}}$  for the WL sequences with the parametrized EOS 2H, HB, and 2B. The plots show that the differences are less than  $2 \times 10^{-4}$ . The compactness increases in the order of 2H, HB, and 2B; the fractional

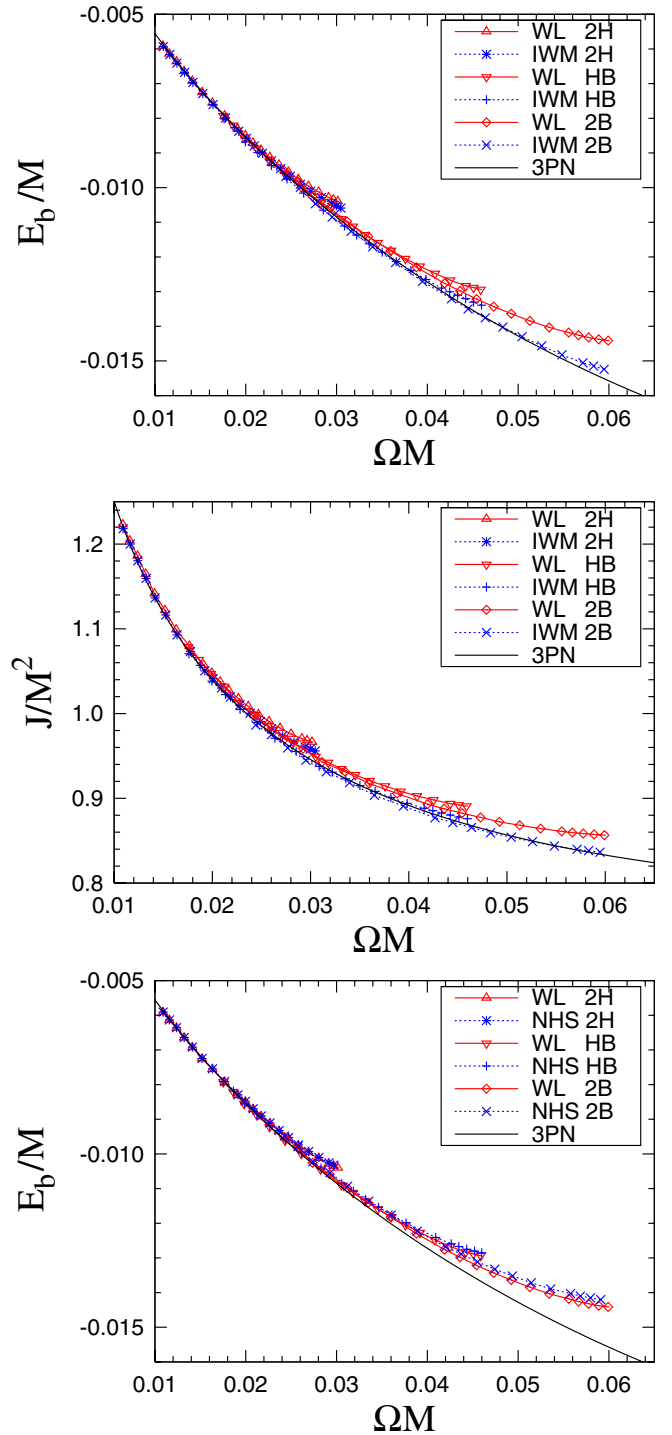


FIG. 3 (color online). Plots of the WL, NHS, and IWM sequences for the parametrized EOS 2H, HB, and 2B. Top panel: Binding energy  $E_b = M_{\text{ADM}} - M$  normalized by  $M = 2M_1$  with respect to the normalized angular velocity  $\Omega M$  of the WL and IWM sequences. Middle panel: Total angular momentum  $J$  normalized by  $M^2$  of the WL and IWM sequences. Bottom panel: Normalized binding energy of the WL and NHS sequences. In each panel, a thin solid curve corresponds to that of the 3PN approximation.

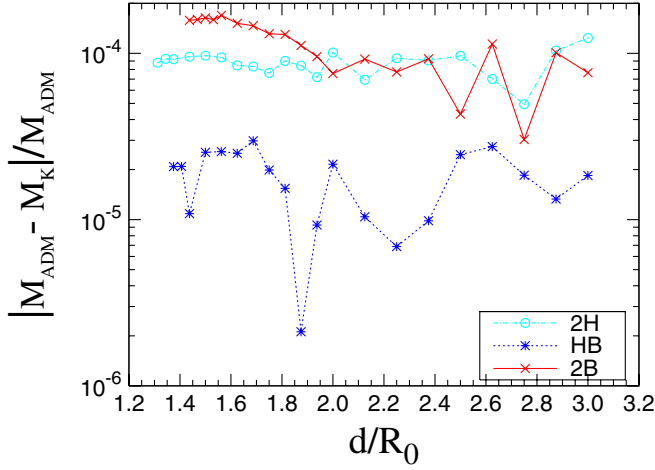


FIG. 4 (color online). Fractional differences of  $M_{\text{ADM}}$  and  $M_K$  with respect to the orbital radius  $d/R_0$  of the WL sequences for parametrized EOS 2H, HB and 2B.

differences, however, do not necessarily increase with increasing compactness in this range  $M_1/R \lesssim 0.2$ . The fact that the fractional difference is well controlled for these sequences is evidence that the binding energy in Fig. 3 is calculated accurately. The virial relation Eq. (54), normalized by  $M_{\text{ADM}}$ , is also calculated to examine the accuracy of the numerical solutions, whose absolute value is about  $0.5 \sim 1$  times that of the fractional difference of two masses.

### C. Quasiequilibrium sequences with four-parameter fitted EOS

In the paper [18], optimal values for the parameters of four-parameter fitted EOS have been derived for 34 candidates of the neutron-star EOS (17 selected EOS of nuclear matter with varied parameters). We choose five representative EOS, which are SLy [41], APR1 [42], FPS [43], BGN1H1 [44], and ALF3 [45]. The first three are made only from normal nuclear matter, while BGN1H1 involves a mixed phase with hyperons, and ALF3 with quarks. For the latter two EOS, the value of  $\Gamma$  becomes smaller in the mixed phase with the exotic matter at a few times above nuclear density [18]. However, BGN1H1 is a stiff EOS having the largest  $p_1$  among them, and hence the core of the mixed phase is not large for the mass  $M_1 = 1.35M_\odot$ .

In Fig. 5, the binding energy  $E_b$  of the WL sequences for these parametrized EOS are plotted. As in the case of the one-parameter parametrized EOS in Sec. IV B, the sequences with higher compactness  $M_1/R$  extend to higher values of  $\Omega M$ . Also, the WL sequences deviate from the 3PN curve at larger  $\Omega M$ . Among these EOS, APR1 is the softest, giving the most compact neutron-star model; and the corresponding binary sequence reaches the highest value,  $\sim 0.058$ , of  $\Omega M$ . However, as seen in the bottom panel of Fig. 5, the binding energy curve of APR1 is slightly off from the 3PN curve even for the smaller  $\Omega M$

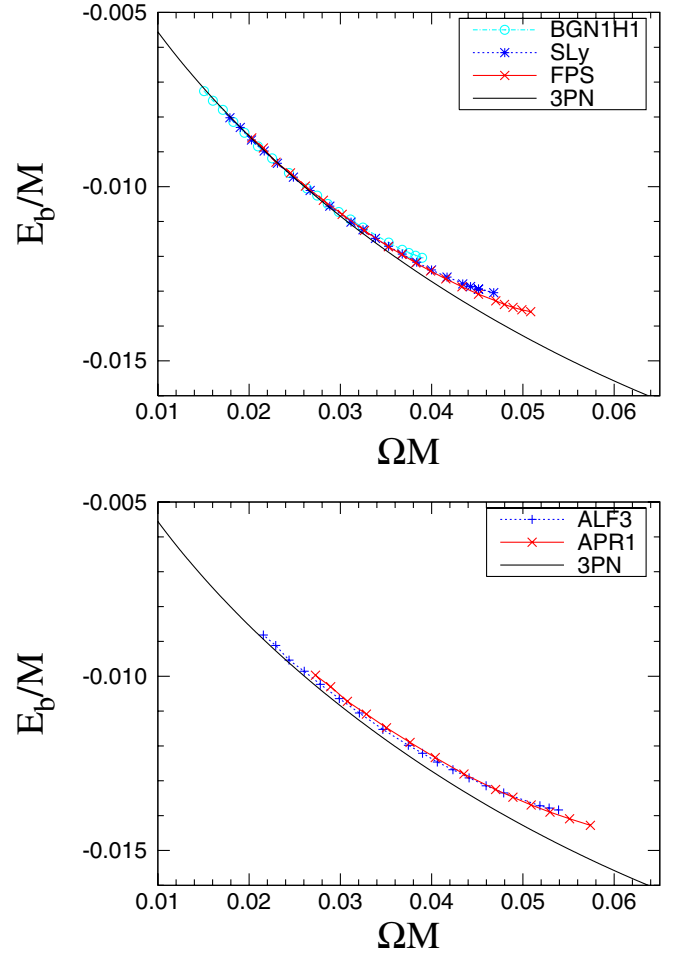


FIG. 5 (color online). Binding energy  $E_b$  of WL sequences for the four-parameter fitted EOS. Top panel: for the EOS, BGN1H1, SLy, and FPS. Bottom panel: for the EOS, ALF3, and APR1.

of the sequence. In our neutron-star code, using a finite difference scheme, the core of the neutron star is covered by fewer grid points in the central coordinates when the binary separation becomes larger and the neutron stars more compact; this may increase the numerical errors. We plan to incorporate a binary computation in the new code [33], in which enough grids are maintained, to densely to cover the neutron star, irrespective of the binary separation or neutron-star radius. The results of the APR1 curve as well as more compact binary sequences will be studied using the new code.

In [15], the gravitational waveform computed from inspiral simulations has been analyzed to estimate the accuracy with which gravitational-wave observations can constrain neutron-star radius, an EOS parameter correlated with the departure from point-particle inspiral. A promising result is that the neutron-star radius can be constrained to  $\delta R \sim 1$  km for an interferometric detector with the sensitivity of Advanced LIGO, in either a broadband configuration or a narrowband with peak sensitivity around

1150 Hz. This suggests that the successful observations of gravitational waves may exclude even a couple of EOS shown in Fig. 5.

#### D. Comparison of the orbital phase in the last several orbits

In this section, we approximately determine the orbital evolution in the late inspiral phase up to the onset of merger using the quasiequilibrium sequences computed in the previous section. To construct a quasiequilibrium sequence, one assumes that each BNS evolves adiabatically along the sequence, that the radial velocity is much smaller than the orbital velocity. Given the rest mass and the EOS, each quasiequilibrium sequence is defined by one parameter: The total energy and angular momentum of the binary system along a sequence are parametrized by the orbital angular velocity as  $E(\Omega)$  and  $J(\Omega)$ .

The time evolution of the angular velocity then becomes

$$\frac{d\Omega}{dt} = \left(\frac{dE}{d\Omega}\right)^{-1} \frac{dE}{dt} \equiv F(\Omega)^{-1}. \quad (55)$$

For the gravitational-wave luminosity,  $dE/dt$ , we adopt the 3.5PN formula for two point masses [46]. Tidal deformation of the neutron stars in close orbits makes the attractive force between two stars stronger, and hence it accelerates the orbital velocity, resulting in the enhancement of the gravitational-wave luminosity. Thus, the 3.5PN formula for the luminosity is likely to underestimate that of the BNS. However, this effect plays an important role only for the last  $\sim 1$  orbit, and for most of the late inspiral orbits, the 3.5PN formula is a good approximation.

Numerical integration of Eq. (55) provides the relation between  $t$  and  $\Omega$  from

$$t = \int d\Omega F(\Omega). \quad (56)$$

From this, the angular velocity as a function of time,  $\Omega(t)$ , is obtained. Using this relation, we can also compute the approximate orbital phase evolution by

$$N = \frac{1}{2\pi} \int \Omega(t) dt. \quad (57)$$

We note that the numerical model with the maximum value of  $\Omega$  for each sequence presented in this paper does not exactly, but does approximately, correspond to a solution at the closest orbit. We stop the integration of Eq. (56) when  $\Omega$  reaches its maximum.

In the top panel of Fig. 6,  $\Omega M$  is plotted as a function of time for EOS 2B, HB, FPS, and SLy in the WL formulation. In the bottom panel of Fig. 6, the results for 2B and HB, calculated in both the WL and IWM formulation, are compared. We also plot the results of two point masses, derived from the Taylor-T4 formula [47].

The top panel of Fig. 6 shows that for the small values of  $\Omega$ , all the curves approximately agree, irrespective of the

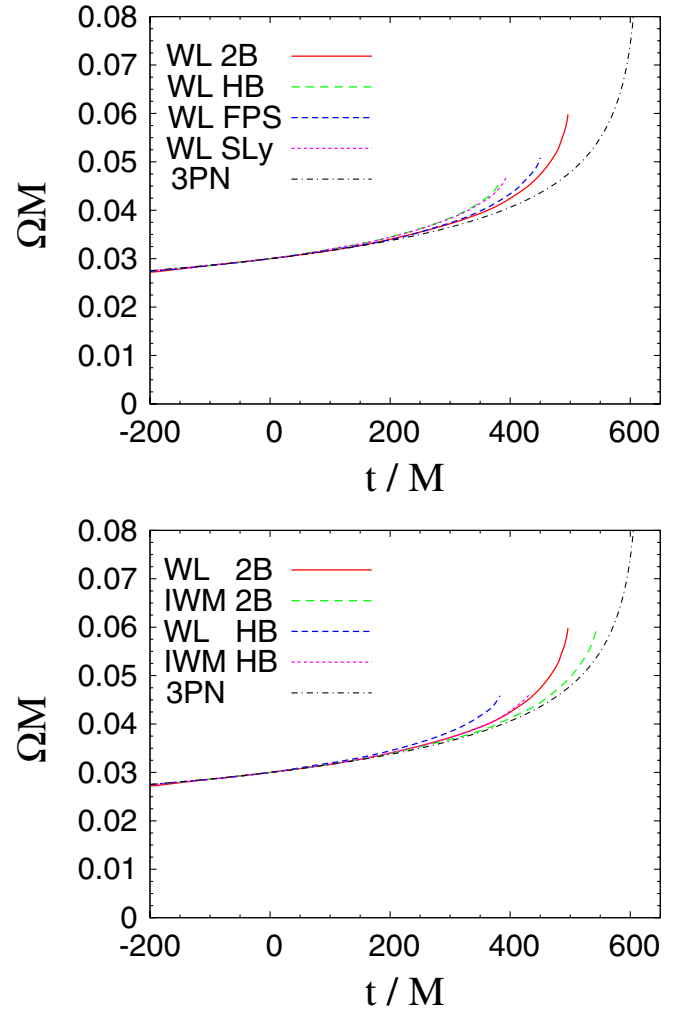


FIG. 6 (color online). Top panel: Orbital angular velocity,  $\Omega$ , as a function of time for EOS 2B, HB, FPS, and SLy of the WL sequences. Bottom panel: Same as the top panel but for EOS 2B and HB of the WL and IWM sequences. For the both panels, the results by the Taylor-T4 formula are also plotted. The units of  $\Omega$  and time are  $M^{-1}$  and  $M$ , respectively. For comparing the results, the time axis is shifted such that  $\Omega M = 0.03$  is aligned at  $t = 0$  for all the curves.

EOS. This is natural because for such small values, tidal deformation does not play an important role and orbital velocity is sufficiently small ( $v < 0.3c$ ) that the post-Newtonian formula (Taylor-T4 formula) with the point-particle approximation should be an excellent approximation.

By contrast, the values of  $\Omega(t)$  computed from the numerical sequences deviate from those given by the Taylor-T4 formula for  $\Omega M \gtrsim 0.035$ – $0.04$ , for all of the EOS and all formulations used to compute the quasiequilibria. This is due to the tidal deformation of the neutron stars; the rate of change of the energy as a function of  $\Omega$  approaches zero for the close orbits, as seen in Figs. 3 and 5. This deviation occurs at more distant orbits for less

compact neutron stars (i.e., for the stiffer EOS), indicating, as expected, that one can extract from the curve  $\Omega(t)$  a characteristic of the component neutron stars related to their compactness and a corresponding parameter of the EOS.

The bottom panel of Fig. 6 shows that the curves  $\Omega(t)$  computed by the WL and IWM formulations are significantly different, as expected from the results of  $E(\Omega)$ . In the case that the IWM formulation is adopted, the merger time is overestimated by  $\sim 50M$ , which is a quite a large factor. This suggests that the results in the IWM formulation do not work well for predicting the evolution of the last several orbits before the onset of merger.

In Fig. 7, we plot the curves of  $N$  as a function of  $\Omega M$ ; the top panel is for EOS 2B, HB, FPS, and SLy in the WL formulation and the bottom for EOS 2B and HB in the WL and IWM formulation. The top panel shows that the number of orbital cycles in the late inspiral phase depends

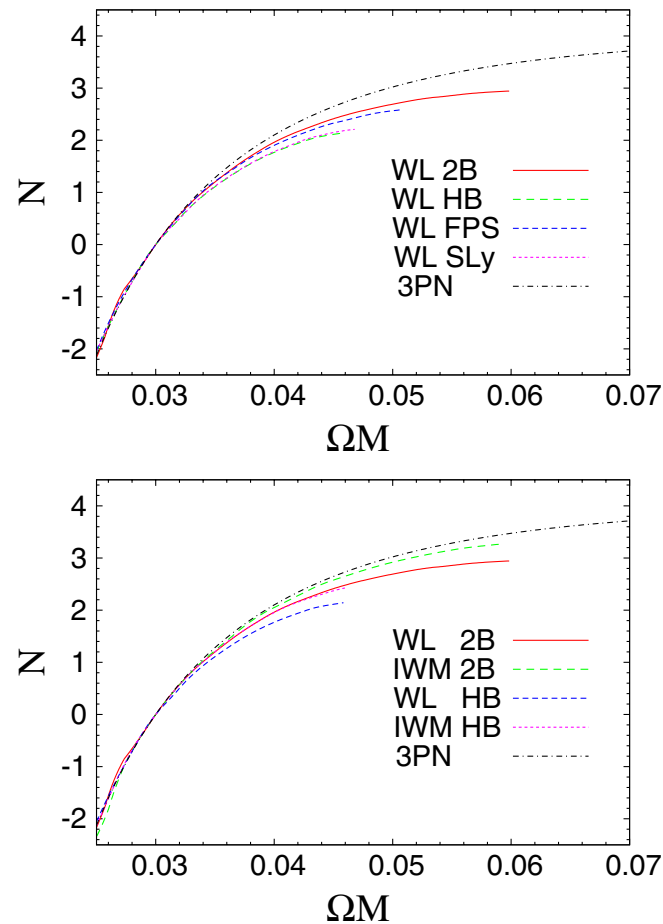


FIG. 7 (color online). Top panel: Orbital cycle,  $N$ , as a function of time for EOS 2B, HB, FPS, and SLy of the WL sequences. Bottom panel: The same as the above but for EOS 2B and HB of the WL and IWM sequences. For the both panels, the results of the Taylor-T4 formula are also plotted. For comparing the results, the time axis is shifted such that  $N = 0$  is aligned at  $\Omega M = 0.03$  for all the curves.

strongly on the EOS. For a soft EOS, e.g., EOS 2B, in which the compactness of the neutron star is largest, the number of cycle is largest. By contrast, for a stiff EOS such as SLy, the number of cycles may be smaller by  $\sim 1$  than that for EOS 2B.

In the bottom panel of Fig. 7, the results for the number of cycle calculated from different formulations are compared. As expected from the results for  $\Omega(t)$ , the IWM formulation overestimates the number of cycles. The error  $\Delta N$  is  $\sim 0.5$  for the EOS 2B; i.e., one cycle of gravitational waves would be overestimated.

## V. DISCUSSION

The deviations of the binding energy and total angular momentum of WL/NHS sequences from the 3PN point-particle sequence as well as from the IWM sequences are likely to be due to the tidal deformation of neutron stars in the binary system coupled with general relativistic effects. As the compactness of the component neutron stars increases, the deviation from the 3PN sequence at a certain value of  $\Omega M$  decreases—WL/NHS sequences become closer to the point-particle sequence, but not by as much as the IWM sequences do. It has been believed that, as the compactness of the component neutron stars increases, the behavior of the binding energy and angular momentum of binary sequences more closely approximates that of point masses. This is found in the results of IWM sequences but to a lesser extent in the WL/NHS sequences. The behavior of the IWM sequence was interpreted as the effacing of the tidal effects due to the strong gravity: that is, as the compactness increases, the sequences of binary neutron-star solutions become much closer to the sequences of two point masses, because the tidal effect is masked by the stronger self-gravity of each component star. However, the results of WL/NHS sequences suggest that such effacing of the tidal effect seen in IWM sequence is an artifact of the conformally flat approximation, at least for the case of equal mass binary neutron stars.

In the WL/NHS formulations, all components of Einstein's equation are solved without approximation on a initial hypersurface, while in the IWM formulation, some terms of second post-Newtonian order are truncated. As discussed in [7] the difference between the IWM and WL/NHS formulations in the binding energy  $E_b$  is estimated at second post-Newtonian order as  $M h_{ab} v^a v^b$ , where the magnitude of the orbital velocity  $v^a$  is typically  $v \sim 0.34(\Omega M/0.04)^{1/3}$ . Since  $h_{ab}$  is  $O(v^4)$ , the order of the difference in the binding energy is given by  $\Delta E_b/M = O(v^6) \sim 10^{-3}$ , and a larger deviation as  $v$  becomes larger for more compact sequences is expected. This estimate is consistent with our results shown in Figs. 3 and 5. Note also that the tidal effect is larger for the EOS with a larger  $\Gamma$  as we used in our computations. So far, our WL/NHS codes have passed several code tests (as have the IWM codes), and results of two independent WL codes agreed for a BNS

sequence with  $M_1/R = 0.17$  as shown in [7]. These results support our argument that the WL/NHS results accurately correct the IWM results. A computation of quasiequilibrium BNS sequences using a totally different numerical method, such as the fully constrained scheme [9], would be a helpful additional check.

We think our results suggest that the circularity of orbit is more accurately enforced on a WL/NHS sequence than a IWM sequence. However, in such quasiequilibrium sequences, some important features of realistic inspirals are ignored. Those include the radial velocity due to gravitational radiation reaction at 2.5PN order that is likely to be comparable to the 2PN terms during the last few orbits where the neutron-star velocity is of order  $v \sim 0.1$ , and a tidal lag angle of about 10–20 degrees that is found in inspiral simulations. Therefore, a caveat is that estimates of the merger time and orbital cycles using quasiequilibrium sequences shown in Sec. IV D involve errors due to ignoring these effects.

Recently, several groups have developed methods to treat the general relativistic tidal deformations analytically [48]. Comparison of these analytic results and the present results for WL/NHS sequences may be useful in calibrating the binding energy or the total angular momentum of the quasiequilibrium sequence in the regime where the relativistic tidal effects become important. Finally, by combining the analytic and numerical results, more accurate quasiequilibrium models for the late inspirals may be constructed [49].

The WL/NHS formulations can be also used to construct models of rotating neutron stars. In [50], axisymmetric rotating relativistic stars are computed using the fully constrained formulation with maximal slicing and the generalized Dirac gauge conditions [9]. Those solutions agreed with the ones calculated using a stationary axisymmetric metric with the additional discrete symmetry of the simultaneous transformation,  $t \rightarrow -t$  and  $\phi \rightarrow -\phi$ . The WL/NHS formulations include more general stationary axisymmetric spacetimes, which do not depend on the additional symmetry. Therefore, the WL/NHS formulations can be applied, for example, to rotating neutron stars that may have both toroidal and poloidal components of the magnetic fields as well as meridional circulation. Even in this case, the WL/NHS formulation can be used to compute exact equilibria that are more general than those calculated in [51]. We plan to extend our codes to compute relativistic rotating stars and binary systems that each include strong magnetic fields.

## ACKNOWLEDGMENTS

This work was supported by JSPS Grants-in-Aid for Scientific Research (C) No. 20540275 and (B) No. 21340051, MEXT Grant-in-Aid for Scientific Research on Innovative Area No. 20105004, NSF Grants No. PHY0071044 and No. PHY0503366, NASA Grant

No. NNG05GB99G, and ANR Grant No. 06-2-134423 *Méthodes mathématiques pour la relativité générale*. K.U. and E.G. acknowledge support from JSPS Invitation Fellowship for Research in Japan (Short-term) and the invitation program of foreign researchers at Paris observatory.

## APPENDIX A: BASIC EQUATIONS

In this Appendix, the system of equations used in WL/NHS codes is presented in detail. The equations include all components of Einstein's equation, the first integral of the relativistic Euler equation, and the rest-mass conservation equation for the irrotational flow. The WL/NHS formulations are based on [9–11].

### 1. Conventions

As mentioned in Sec. II A, the 3 + 1 decomposition is applied to the spacetime  $\mathcal{M}$  in the WL/NHS formulations. First, several definitions for the quantities relating to the spatial geometry are introduced.

#### a. Connections

The spatial metric  $\gamma_{ab}$ , a conformally rescaled spatial metric  $\tilde{\gamma}_{ab}$ , and a flat metric  $f_{ab}$  are associated with the derivatives  $D_a$ ,  $\tilde{D}_a$ , and  $\overset{\circ}{D}_a$ , respectively. We introduce the conformal rescaling by  $\gamma_{ab} = \psi^4 \tilde{\gamma}_{ab}$ , whose determinant  $\tilde{\gamma}$  is equal to that of the flat metric  $f$ ,  $\tilde{\gamma} = f$ , to specify the decomposition of the spatial metric uniquely. Covariant derivatives  $D_a$  and  $\tilde{D}_a$  are related by

$$D_b X^a = \tilde{D}_b X^a + \tilde{C}_{bc}^a X^c, \quad (\text{A1})$$

where  $X^a$  is a spatial vector, and a coefficient  $\tilde{C}_{ab}^c$  is written

$$\begin{aligned} \tilde{C}_{ab}^c &= \frac{1}{2} \gamma^{cd} (\tilde{D}_a \gamma_{db} + \tilde{D}_b \gamma_{ad} - \tilde{D}_d \gamma_{ab}) \\ &= \frac{2}{\psi} (\tilde{\gamma}^c_b \tilde{D}_a \psi + \tilde{\gamma}^c_a \tilde{D}_b \psi - \tilde{\gamma}_{ab} \tilde{\gamma}^{cd} \tilde{D}_d \psi). \end{aligned} \quad (\text{A2})$$

Also,  $\tilde{D}_a$  and  $\overset{\circ}{D}_a$  are related by

$$\tilde{D}_b X^a = \overset{\circ}{D}_b X^a + C_{bc}^a X^c, \quad (\text{A3})$$

where  $C_{ab}^c$  is written

$$\begin{aligned} C_{ab}^c &= \frac{1}{2} \tilde{\gamma}^{cd} (\overset{\circ}{D}_a \tilde{\gamma}_{db} + \overset{\circ}{D}_b \tilde{\gamma}_{ad} - \overset{\circ}{D}_d \tilde{\gamma}_{ab}) \\ &= \frac{1}{2} \tilde{\gamma}^{cd} (\overset{\circ}{D}_a h_{db} + \overset{\circ}{D}_b h_{ad} - \overset{\circ}{D}_d h_{ab}). \end{aligned} \quad (\text{A4})$$

A trace of  $C_{ab}^c$

$$C_{ba}^b = \frac{1}{2} \tilde{\gamma}^{bc} \overset{\circ}{D}_a \tilde{\gamma}_{bc} = \frac{1}{\sqrt{\tilde{\gamma}}} \overset{\circ}{D}_a \sqrt{\tilde{\gamma}}, \quad (\text{A5})$$

and the condition  $\tilde{\gamma} = f$  that specifies the conformal de-

composition imply  $C_{ca}^c = 0$  and hence  $\tilde{D}_a \psi = \overset{\circ}{D}_a \psi$ . The relations

$$\tilde{\gamma}^{ab} C_{ab}^c + \tilde{\gamma}^{bc} C_{ab}^c + \overset{\circ}{D}_a \tilde{\gamma}^{ac} = 0 \quad (\text{A6})$$

and  $\tilde{\gamma} = f$ , and the Dirac gauge condition  $\overset{\circ}{D}_b \tilde{\gamma}^{ab} = 0$  imply  $\tilde{\gamma}^{ab} C_{ab}^c = 0$ .

### b. Conformally rescaled extrinsic curvatures

The form of the extrinsic curvature  $K_{ab}$  is discussed in Sec. II B. In the equations for our numerical code, it is decomposed in terms of the trace  $K = \gamma^{ab} K_{ab}$  and the tracefree part  $A_{ab}$ ,

$$K_{ab} = A_{ab} + \frac{1}{3} \gamma_{ab} K. \quad (\text{A7})$$

The conformally rescaled tracefree part  $\tilde{A}_a{}^b$  is defined as

$$\tilde{A}_a{}^b = A_a{}^b, \quad (\text{A8})$$

and its index is lowered (raised) by  $\tilde{\gamma}_{ab}$  ( $\tilde{\gamma}^{ab}$ ).

We define  $L_X \gamma_{ab}$  as the tracefree part of  $\mathfrak{L}_X \gamma_{ab}$ , where  $X^a$  is a spatial vector on  $\Sigma_t$ ,

$$L_X \gamma_{ab} = \mathfrak{L}_X \gamma_{ab} - \frac{1}{3} \gamma_{ab} \gamma^{cd} \mathfrak{L}_X \gamma_{cd} \quad (\text{A9})$$

$$= D_a X_b + D_b X_a - \frac{2}{3} \gamma_{ab} D_c X^c. \quad (\text{A10})$$

The r.h.s. of this equation is a conformal Killing operator, and its conformally rescaled version is defined by

$$\tilde{L}_X \tilde{\gamma}_{ab} = \psi^4 L_X \gamma_{ab}. \quad (\text{A11})$$

Note that a vector is rescaled,  $\tilde{X}^a = X^a$ , and  $\tilde{\gamma}_{ab}$  is used when lowering the index of the rescaled vector.

When helical symmetry,  $\mathfrak{L}_k g_{\alpha\beta} = 0$ , is imposed as in Sec. II B, the tensors  $A_{ab}$  and  $\tilde{A}_{ab}$  have the forms

$$A_{ab} = \frac{1}{2\alpha} L_\omega \gamma_{ab} \quad \text{and} \quad \tilde{A}_{ab} = \frac{1}{2\alpha} \tilde{L}_\omega \tilde{\gamma}_{ab}, \quad (\text{A12})$$

respectively; while for the WL formulation,

$$A_{ab} = \frac{1}{2\alpha} L_\beta \gamma_{ab} \quad \text{and} \quad \tilde{A}_{ab} = \frac{1}{2\alpha} \tilde{L}_\beta \tilde{\gamma}_{ab}. \quad (\text{A13})$$

The following expression for the conformally rescaled  $\tilde{A}_{ab}$  is used later,

$$\begin{aligned} \tilde{A}_a{}^b &= \frac{1}{2\alpha} \left( \tilde{D}_a \tilde{\beta}^b + \tilde{D}^b \tilde{\beta}_a - \frac{2}{3} \tilde{\gamma}_a{}^b \tilde{D}_c \tilde{\beta}^c \right) \\ &\quad + \frac{1}{2\alpha} \Omega \tilde{\gamma}^{bc} \tilde{L}_\phi \tilde{\gamma}_{ac}. \end{aligned} \quad (\text{A14})$$

The last term in the above

$$\tilde{L}_\phi \tilde{\gamma}_{ab} = \mathfrak{L}_\phi \tilde{\gamma}_{ab} - \frac{1}{3} \tilde{\gamma}_{ab} \tilde{\gamma}^{cd} \mathfrak{L}_\phi \tilde{\gamma}_{cd} \quad (\text{A15})$$

$$= \tilde{D}_a \tilde{\phi}_b + \tilde{D}_b \tilde{\phi}_a - \frac{2}{3} \tilde{\gamma}_{ab} \tilde{D}_c \tilde{\phi}^c, \quad (\text{A16})$$

with  $\tilde{\phi}^a = \phi^a$  and  $\tilde{\phi}_a := \tilde{\gamma}_{ab} \tilde{\phi}^b$ , appears only in the helically symmetric case and is eliminated when the WL formulation is used.

### c. Conformally rescaled intrinsic quantities

The Ricci tensor  ${}^3R_{ab}$  of the spacelike hypersurface  $\Sigma_t$  associated with the spatial metric  $\gamma_{ab}$  is decomposed into terms related to the conformal factor  $\psi$ ,  ${}^3\tilde{R}_{ab}^\psi$ , and the conformal Ricci tensor  ${}^3\tilde{R}_{ab}$  associated with  $\tilde{\gamma}_{ab}$ :

$${}^3R_{ab} = {}^3\tilde{R}_{ab}^\psi + {}^3\tilde{R}_{ab}. \quad (\text{A17})$$

The first term is written

$$\begin{aligned} {}^3\tilde{R}_{ab}^\psi &= -\frac{2}{\psi} \tilde{D}_a \tilde{D}_b \psi - \tilde{\gamma}_{ab} \frac{2}{\psi} \tilde{D}^c \tilde{D}_c \psi + \frac{6}{\psi^2} \tilde{D}_a \psi \tilde{D}_b \psi \\ &\quad - \tilde{\gamma}_{ab} \frac{2}{\psi^2} \tilde{D}_c \psi \tilde{D}^c \psi. \end{aligned} \quad (\text{A18})$$

In  ${}^3\tilde{R}_{ab}$ , terms linear in  $h_{ab}$  or  $h^{ab}$  are separated as

$${}^3\tilde{R}_{ab} = -\frac{1}{2} \overset{\circ}{D}^c \overset{\circ}{D}_c h_{ab} + \tilde{R}_{ab}^D + \tilde{R}_{ab}^{\text{NL}}, \quad (\text{A19})$$

where  $\tilde{R}_{ab}^D$  includes terms linear in the conformal metric in the form of flat divergences

$$\tilde{R}_{ab}^D = -\frac{1}{2} (f_{ac} \overset{\circ}{D}_b F^c + f_{bc} \overset{\circ}{D}_a F^c), \quad (\text{A20})$$

$$F^a := \overset{\circ}{D}_b \tilde{\gamma}^{ab} = \overset{\circ}{D}_b h^{ab}; \quad (\text{A21})$$

nonlinear terms,  $\tilde{R}_{ab}^{\text{NL}}$ , are written

$$\begin{aligned} \tilde{R}_{ab}^{\text{NL}} &= -\frac{1}{2} (\overset{\circ}{D}_b h^{cd} \overset{\circ}{D}_c h_{ad} + \overset{\circ}{D}_a h^{cd} \overset{\circ}{D}_c h_{bd} \\ &\quad + h^{cd} \overset{\circ}{D}_c \overset{\circ}{D}_d h_{ab}) - \overset{\circ}{D}_a C_{cb}^c + C_{ab}^c C_{dc}^d - C_{ac}^d C_{bd}^c \\ &\quad - \frac{1}{2} [\overset{\circ}{D}_b (h_{ac} F^c) + \overset{\circ}{D}_a (h_{bc} F^c)] + F^c C_{c,ab}, \end{aligned} \quad (\text{A22})$$

where  $C_{c,ab} := \tilde{\gamma}_{cd} C_{ab}^d$ . The above expression for  $\tilde{R}_{ab}^{\text{NL}}$  can be simplified by applying the condition  $\tilde{\gamma} = f$  and the generalized Dirac gauge condition, implying  $C_{ba}^b = 0$  and  $F^a = 0$ .

The Ricci scalar curvature  ${}^3R$  of  $\Sigma_t$  is related to the conformal Ricci scalar  ${}^3\tilde{R} := \tilde{\gamma}^{ab} {}^3\tilde{R}_{ab}$  by

$${}^3R = \frac{1}{\psi^4} {}^3\tilde{R} - \frac{8}{\psi^5} \tilde{D}^a \tilde{D}_a \psi. \quad (\text{A23})$$

## 2. Equations for the gravitational fields

Equations used in the numerical code are shown below. Although we impose the gauge conditions (12) and (13),

the following equations are not restricted to these choices. The conformal decomposition, however, is specified by a condition  $\tilde{\gamma} = f$  that is used, for example, to obtain the relation  $\tilde{D}_a \psi = \overset{\circ}{D}_a \psi$ .

### a. Hamiltonian constraint

The projection of Einstein's equation along the normal  $n^\alpha$  to the hypersurface yields

$$(G_{\alpha\beta} - 8\pi T_{\alpha\beta})n^\alpha n^\beta = \frac{1}{2}({}^3R + K^2 - K_{ab}K^{ab} - 16\pi\rho_H) = 0. \quad (\text{A24})$$

Substituting Eq. (A23), we have

$$(G_{\alpha\beta} - 8\pi T_{\alpha\beta})n^\alpha n^\beta = \frac{4}{\psi^5} \left[ -\tilde{D}^a \tilde{D}_a \psi + \frac{\psi}{8} {}^3\tilde{R} - \frac{\psi^5}{8} \left( \tilde{A}_{ab} \tilde{A}^{ab} - \frac{2}{3} K^2 \right) - 2\pi\psi^5 \rho_H \right] = 0. \quad (\text{A25})$$

The above equation is rewritten to isolate the flat Laplacian  $\overset{\circ}{\Delta} \psi := \overset{\circ}{D}^a \overset{\circ}{D}_a \psi$  on the left-hand side, and the other terms are treated as a source on the r.h.s.,

$$\overset{\circ}{\Delta} \psi = \mathcal{S}_H \quad (\text{A26})$$

with the source  $\mathcal{S}_H$  given by

$$\mathcal{S}_H = -h^{ab} \overset{\circ}{D}_a \overset{\circ}{D}_b \psi + \tilde{\gamma}^{ab} C_{ab}^c \overset{\circ}{D}_c \psi + \frac{\psi}{8} {}^3\tilde{R} - \frac{\psi^5}{8} \left( \tilde{A}_{ab} \tilde{A}^{ab} - \frac{2}{3} K^2 \right) - 2\pi\psi^5 \rho_H. \quad (\text{A27})$$

### b. Momentum constraint

The momentum constraint is written in an elliptic equation to be solved for the covariant component of the conformally rescaled nonrotating shift  $\tilde{\beta}_a := \tilde{\gamma}_{ab} \beta^b$ . We begin with

$$(G_{\alpha\beta} - 8\pi T_{\alpha\beta})\gamma_a^\alpha n^\beta = -D_b K_a^b + D_a K + 8\pi j_a = -\frac{1}{\psi^6} \tilde{D}_b (\psi^6 \tilde{A}_a^b) + \frac{2}{3} \tilde{D}_a K + 8\pi j_a = 0, \quad (\text{A28})$$

then substitute Eq. (A14) and a relation

$$\tilde{D}_b \tilde{D}_a \beta^b - \tilde{D}_a \tilde{D}_b \beta^b = {}^3\tilde{R}_{ab} \beta^b, \quad (\text{A29})$$

to obtain

$$\tilde{D}_b \tilde{D}^b \tilde{\beta}_a + \frac{1}{3} \tilde{D}_a \tilde{D}_b \tilde{\beta}^b + {}^3\tilde{R}_{ab} \tilde{\beta}^b + \Omega \tilde{D}_b (\tilde{L}\phi)_a^b + 2\alpha \tilde{A}_a^b \frac{\alpha}{\psi^6} \tilde{D}_b \left( \frac{\psi^6}{\alpha} \right) - \frac{4}{3} \alpha \tilde{D}_a K - 16\pi \alpha j_a = 0. \quad (\text{A30})$$

From the first two terms of the r.h.s. of Eq. (A30), the flat terms  $\overset{\circ}{\Delta} \tilde{\beta}_a + \frac{1}{3} \overset{\circ}{D}_a \overset{\circ}{D}^b \tilde{\beta}_b$  are similarly isolated,

$$\begin{aligned} \tilde{D}_b \tilde{D}^b \tilde{\beta}_a + \frac{1}{3} \tilde{D}_a \tilde{D}_b \tilde{\beta}^b &= \overset{\circ}{\Delta} \tilde{\beta}_a + \frac{1}{3} \overset{\circ}{D}_a \overset{\circ}{D}^b \tilde{\beta}_b + h^{bc} \overset{\circ}{D}_b \overset{\circ}{D}_c \tilde{\beta}_a \\ &\quad - \tilde{\gamma}^{bc} \overset{\circ}{D}_b (C_{ca}^d \tilde{\beta}_d) - \tilde{\gamma}^{bc} C_{bc}^d \tilde{D}_d \tilde{\beta}_a - \tilde{\gamma}^{bc} C_{ba}^d \tilde{D}_c \tilde{\beta}_d \\ &\quad + \frac{1}{3} \overset{\circ}{D}_a (h^{bc} \overset{\circ}{D}_b \tilde{\beta}_c - \tilde{\gamma}^{bc} C_{bc}^d \tilde{\beta}_d). \end{aligned} \quad (\text{A31})$$

We keep  $\tilde{D}_a$  instead of replacing it by  $\overset{\circ}{D}_a$  and a connection  $C_{ab}^c$  in a couple of terms in the Eq. (A31), to shorten the equation. A decomposition proposed by Shibata,

$$\tilde{\beta}_a = G_a + \frac{1}{8} \overset{\circ}{D}_a (B - x^b G_b), \quad \text{where } \overset{\circ}{D}_a x^b = \delta_a^b, \quad (\text{A32})$$

is substituted in the expression for the flat operator  $\overset{\circ}{\Delta} \tilde{\beta}_a + \frac{1}{3} \overset{\circ}{D}_a \overset{\circ}{D}^b \tilde{\beta}_b$ ,

$$\overset{\circ}{\Delta} \tilde{\beta}_a + \frac{1}{3} \overset{\circ}{D}_a \overset{\circ}{D}^b \tilde{\beta}_b = \overset{\circ}{\Delta} G_a + \frac{1}{6} \overset{\circ}{D}_a (\overset{\circ}{\Delta} B - x^b \overset{\circ}{\Delta} G_b), \quad (\text{A33})$$

to obtain elliptic equations that are solved simultaneously,

$$\overset{\circ}{\Delta} G_a = \mathcal{S}_a, \quad (\text{A34})$$

$$\overset{\circ}{\Delta} B = x^a \mathcal{S}_a, \quad (\text{A35})$$

where the source  $\mathcal{S}_a$  is written

$$\begin{aligned} \mathcal{S}_a := & -h^{bc} \overset{\circ}{D}_b \overset{\circ}{D}_c \tilde{\beta}_a + \tilde{\gamma}^{bc} \overset{\circ}{D}_b (C_{ca}^d \tilde{\beta}_d) + \tilde{\gamma}^{bc} C_{bc}^d \tilde{D}_d \tilde{\beta}_a \\ & + \tilde{\gamma}^{bc} C_{ba}^d \tilde{D}_c \tilde{\beta}_d - \frac{1}{3} \overset{\circ}{D}_a (h^{bc} \overset{\circ}{D}_b \tilde{\beta}_c - \tilde{\gamma}^{bc} C_{bc}^d \tilde{\beta}_d) \\ & - {}^3\tilde{R}_{ab} \tilde{\beta}^b - \Omega \tilde{D}^b \tilde{L}_\phi \tilde{\gamma}_{ab} - 2\alpha \tilde{A}_a^b \frac{\alpha}{\psi^6} \tilde{D}_b \left( \frac{\psi^6}{\alpha} \right) \\ & + \frac{4}{3} \alpha \tilde{D}_a K + 16\pi \alpha j_a. \end{aligned} \quad (\text{A36})$$

A term  $\tilde{D}^b \tilde{L}_\phi \tilde{\gamma}_{ab}$  is computed from

$$\begin{aligned} \tilde{D}^b \tilde{L}_\phi \tilde{\gamma}_{ab} &= \tilde{\gamma}^{bc} \overset{\circ}{D}_c \tilde{L}_\phi \tilde{\gamma}_{ab} - C_{ba}^c \tilde{\gamma}^{bd} \tilde{L}_\phi \tilde{\gamma}_{cd} \\ &\quad + \overset{\circ}{D}_c \tilde{\gamma}^{cb} \tilde{L}_\phi \tilde{\gamma}_{ab} + C_{ac}^d \tilde{\gamma}^{cb} \tilde{L}_\phi \tilde{\gamma}_{ab}, \end{aligned} \quad (\text{A37})$$

which is dropped when the WL formulation is used (see Sec. II B).

### c. Spatial trace part of Einstein's equation

The spatial trace of Einstein's equation is combined with the Hamiltonian constraint,

$$\begin{aligned} & (G_{\alpha\beta} - 8\pi T_{\alpha\beta}) \left( \gamma^{\alpha\beta} + \frac{1}{2} n^\alpha n^\beta \right) \\ &= -\frac{1}{4} {}^3R + \frac{2}{\alpha} D^a D_a \alpha + 2\xi_n K \\ & \quad - \frac{1}{4} (K^2 + 7K_{ab}K^{ab}) - 4\pi(\rho_H + 2S) = 0, \end{aligned} \quad (\text{A38})$$

and it is solved for the combination  $\alpha\psi$ . Using a relation,

$$-\frac{1}{4} {}^3R + \frac{2}{\alpha} D^a D_a \alpha = \frac{2}{\alpha\psi^5} \left[ \tilde{D}^a \tilde{D}_a (\alpha\psi) - \frac{\alpha\psi}{8} {}^3\tilde{R} \right], \quad (\text{A39})$$

and applying helical symmetry, the above equation is rewritten

$$\begin{aligned} & (G_{\alpha\beta} - 8\pi T_{\alpha\beta}) \left( \gamma^{\alpha\beta} + \frac{1}{2} n^\alpha n^\beta \right) \\ &= \frac{2}{\alpha\psi^5} \left[ \tilde{D}^a \tilde{D}_a (\alpha\psi) - \frac{\alpha\psi}{8} {}^3\tilde{R} - \psi^5 \xi_\omega K \right. \\ & \quad \left. - \alpha\psi^5 \left( \frac{7}{8} \tilde{A}_{ab} \tilde{A}^{ab} + \frac{5}{12} K^2 \right) - 2\pi\alpha\psi^5 (\rho_H + 2S) \right] = 0. \end{aligned} \quad (\text{A40})$$

Isolating the flat part  $\overset{\circ}{\Delta}(\alpha\psi)$ , an elliptic equation is derived

$$\overset{\circ}{\Delta}(\alpha\psi) = \mathcal{S}_{\text{tr}}, \quad (\text{A41})$$

where the source  $\mathcal{S}_{\text{tr}}$  is written

$$\begin{aligned} \mathcal{S}_{\text{tr}} := & -h^{ab} \overset{\circ}{D}_a \overset{\circ}{D}_b + \tilde{\gamma}^{ab} C_{ab}^c \overset{\circ}{D}_c (\alpha\psi) + \frac{\alpha\psi}{8} {}^3\tilde{R} \\ & + \psi^5 \xi_\omega K + \alpha\psi^5 \left( \frac{7}{8} \tilde{A}_{ab} \tilde{A}^{ab} + \frac{5}{12} K^2 \right) \\ & + 2\pi\alpha\psi^5 (\rho_H + 2S). \end{aligned} \quad (\text{A42})$$

### d. Spatial tracefree part of Einstein's equation

The projection of Einstein's equation to the initial hypersurface  $\Sigma_t$  is written

$$\begin{aligned} & (G_{\alpha\beta} - 8\pi T_{\alpha\beta}) \gamma_a^\alpha \gamma_b^\beta \\ &= -\xi_n K_{ab} + \gamma_{ab} \xi_n K + {}^3R_{ab} - \frac{1}{2} \gamma_{ab} {}^3R + KK_{ab} \\ & \quad - 2K_{ac} K_b^c - \frac{1}{2} \gamma_{ab} (K^2 + K_{cd} K^{cd}) \\ & \quad - \frac{1}{\alpha} (D_a D_b \alpha - \gamma_{ab} D^c D_c \alpha) - 8\pi S_{ab}. \end{aligned} \quad (\text{A43})$$

The equation to solve for the nonconformal part of the spatial metric  $h_{ab}$  is derived from the tracefree part of the above Eq. (A43). The tracefree operation eliminates terms proportional to  $\gamma_{ab}$ . Applying helical symmetry, (16) and (17), the tracefree part of Eq. (A43) is written

$$(G_{\alpha\beta} - 8\pi T_{\alpha\beta}) \left( \gamma_a^\alpha \gamma_b^\beta - \frac{1}{3} \gamma_{ab} \gamma^{\alpha\beta} \right) = \mathcal{E}_{ab}^{\text{TF}} = 0, \quad (\text{A44})$$

where  $\mathcal{E}_{ab}$  is defined by

$$\begin{aligned} \mathcal{E}_{ab} := & \frac{1}{\alpha} \xi_\omega K_{ab} + {}^3R_{ab} - \frac{1}{\alpha} D_a D_b \alpha \\ & + KK_{ab} - 2K_{ac} K_b^c - 8\pi S_{ab}, \end{aligned} \quad (\text{A45})$$

and  $\mathcal{E}_{ab}^{\text{TF}}$  is its trace free part

$$\begin{aligned} \mathcal{E}_{ab}^{\text{TF}} := & \left( \gamma_a^c \gamma_b^d - \frac{1}{3} \gamma_{ab} \gamma^{cd} \right) \mathcal{E}_{cd} \\ & = \left( \tilde{\gamma}_a^c \tilde{\gamma}_b^d - \frac{1}{3} \tilde{\gamma}_{ab} \tilde{\gamma}^{cd} \right) \mathcal{E}_{cd}. \end{aligned} \quad (\text{A46})$$

The tracefree part of the tensors are also denoted by superscripts TF, hereafter. We further eliminate terms proportional to  $\gamma_{ab}$  remaining in this expression for  $\mathcal{E}_{ab}$  later in this section.

We derive two different equations to solve for  $h_{ab}$ . One is an elliptic equation in which  $\overset{\circ}{\Delta}h_{ab}$  is separated from  ${}^3R_{ab}$  as in Eq. (A19); it is used for both the WL/NHS formulation. The other is for the NHS formulation in which an operator  $(\overset{\circ}{\Delta} - \Omega^2 \partial_\phi^2)h_{ab}$  is separated. The  $\phi$  derivative term in this operator is separated from a term  $\frac{1}{\alpha} \xi_\omega K_{ab}$ , which is derived by applying helical symmetry, (16) and (17), to the time derivatives. For the former equation, the above  $\mathcal{E}_{ab}$  is rewritten

$$\begin{aligned} \mathcal{E}_{ab} = & -\frac{1}{2} \overset{\circ}{\Delta}h_{ab} + \tilde{R}_{ab}^{\text{D}} + \tilde{R}_{ab}^{\text{NL}} + {}^3\tilde{R}_{ab}^\psi - \frac{1}{\alpha} D_a D_b \alpha \\ & + KK_{ab} - 2K_{ac} K_b^c + \frac{1}{\alpha} \xi_\omega K_{ab} - 8\pi S_{ab}, \end{aligned} \quad (\text{A47})$$

and for the latter,

$$\begin{aligned} \mathcal{E}_{ab} = & -\frac{1}{2} (\overset{\circ}{\Delta} - \Omega^2 \partial_\phi^2) h_{ab} + \tilde{R}_{ab}^{\text{D}} + \tilde{R}_{ab}^{\text{NL}} + {}^3\tilde{R}_{ab}^\psi \\ & - \frac{1}{\alpha} D_a D_b \alpha + KK_{ab} - 2K_{ac} K_b^c \\ & + \frac{1}{\alpha} \xi_\omega K_{ab} - \frac{1}{2} \Omega^2 \partial_\phi^2 h_{ab} - 8\pi S_{ab}. \end{aligned} \quad (\text{A48})$$

Terms proportional to  $\gamma_{ab}$  in Eqs. (A47) and (A48) are now eliminated further to simplify the equations. Introducing barred quantities,

$${}^3\bar{R}_{ab}^\psi = -\frac{2}{\psi}\bar{D}_a\bar{D}_b\psi + \frac{6}{\psi^2}\bar{D}_a\psi\bar{D}_b\psi, \quad (\text{A49})$$

$$\bar{D}_a\bar{D}_b\alpha = \overset{\circ}{D}_a\overset{\circ}{D}_b\alpha - C_{ab}^c\overset{\circ}{D}_c\alpha - \frac{2}{\psi}(\overset{\circ}{D}_a\overset{\circ}{D}_b\psi + \overset{\circ}{D}_b\alpha\overset{\circ}{D}_a\psi), \quad (\text{A50})$$

their combination becomes

$$\begin{aligned} & {}^3\bar{R}_{ab}^\psi - \frac{1}{\alpha}\bar{D}_a\bar{D}_b\alpha \\ &= -\frac{1}{\alpha\psi^2}\overset{\circ}{D}_a\overset{\circ}{D}_b(\alpha\psi^2) + \frac{1}{\alpha\psi^2}C_{ab}^c\overset{\circ}{D}_c(\alpha\psi^2) \\ &+ \frac{4}{\alpha\psi^2}[\overset{\circ}{D}_a(\alpha\psi)\overset{\circ}{D}_b\psi + \overset{\circ}{D}_b(\alpha\psi)\overset{\circ}{D}_a\psi], \end{aligned} \quad (\text{A51})$$

which satisfies

$$\left({}^3\bar{R}_{ab}^\psi - \frac{1}{\alpha}D_aD_b\alpha\right)^{\text{TF}} = \left({}^3\bar{R}_{ab}^\psi - \frac{1}{\alpha}\bar{D}_a\bar{D}_b\alpha\right)^{\text{TF}}. \quad (\text{A52})$$

Next, substituting  $K_{ab} = A_{ab} + \frac{1}{3}\gamma_{ab}K$  to terms relating to  $K_{ab}$ , their tracefree part satisfies

$$\begin{aligned} & \left(KK_{ab} - 2K_{ac}K_b{}^c + \frac{1}{\alpha}\mathfrak{L}_\omega K_{ab}\right)^{\text{TF}} \\ &= \left(\frac{1}{3}KA_{ab} - 2A_{ac}A_b{}^c + \frac{1}{\alpha}\mathfrak{L}_\omega A_{ab}\right)^{\text{TF}}. \end{aligned} \quad (\text{A53})$$

For the matter source term,

$$S_{ab} = T_{\alpha\beta}\gamma_a{}^\alpha\gamma_b{}^\beta = (\epsilon + p)u_a u_b + \gamma_{ab}p, \quad (\text{A54})$$

where  $u_a := \gamma_a{}^\alpha u_\alpha$ . We also introduce a barred quantity

$$\bar{S}_{ab} := \rho h u_a u_b, \quad (\text{A55})$$

that satisfies  $S_{ab}^{\text{TF}} = \bar{S}_{ab}^{\text{TF}}$ , where  $h = (\epsilon + p)/\rho$  is used. The tracefree operation to the operator  $(\overset{\circ}{\Delta} - \Omega^2\partial_\phi^2)h_{cd}$  is written

$$\begin{aligned} & -\frac{1}{2}\left(\tilde{\gamma}_a{}^c\tilde{\gamma}_b{}^d - \frac{1}{3}\tilde{\gamma}_{ab}\tilde{\gamma}^{cd}\right)\overset{\circ}{\Delta}h_{cd} \\ &= -\frac{1}{2}\left[\overset{\circ}{\Delta}h_{ab} - \Omega^2\partial_\phi^2 h_{ab} + \frac{1}{3}\tilde{\gamma}_{ab}\overset{\circ}{D}^e h^{cd}\overset{\circ}{D}_e h_{cd}\right. \\ & \quad \left. - \frac{1}{3}\tilde{\gamma}_{ab}\Omega^2\partial_\phi h^{cd}\partial_\phi h_{cd}\right], \end{aligned} \quad (\text{A56})$$

where relations  $\tilde{\gamma}^{cd}\overset{\circ}{D}_e h_{cd} = \tilde{\gamma}^{cd}\partial_\phi h_{cd} = 0$  implied by  $\tilde{\gamma} = f$  is used. The same operation to the Laplacian is written similarly as above, but without  $\partial_\phi$  terms.

Finally, the trace free part  $\mathcal{E}_{ab}^{\text{TF}} = 0$  results in the following elliptic equation,

$$\overset{\circ}{\Delta}h_{ab} = S_{ab}, \quad (\text{A57})$$

where the source  $S_{ab}$  is defined by

$$S_{ab} := 2\bar{\mathcal{E}}_{ab}^{\text{TF}} - \frac{1}{3}\tilde{\gamma}_{ab}\overset{\circ}{D}^e h^{cd}\overset{\circ}{D}_e h_{cd}, \quad (\text{A58})$$

and  $\bar{\mathcal{E}}_{ab}^{\text{TF}}$  is a tracefree part of  $\bar{\mathcal{E}}_{ab}$ , which is written using the rescaled  $\tilde{A}_{ab}$ ,

$$\begin{aligned} \bar{\mathcal{E}}_{ab} &:= \tilde{R}_{ab}^{\text{D}} + \tilde{R}_{ab}^{\text{NL}} + {}^3\bar{R}_{ab}^\psi - \frac{1}{\alpha}\bar{D}_a\bar{D}_b\alpha + \frac{1}{3}\psi^4 K\tilde{A}_{ab} \\ & - 2\psi^4\tilde{A}_{ac}\tilde{A}_b{}^c + \frac{1}{\alpha}\mathfrak{L}_\omega(\psi^4\tilde{A}_{ab}) - 8\pi\bar{S}_{ab}. \end{aligned} \quad (\text{A59})$$

For the equation with the operator  $\overset{\circ}{\Delta} - \Omega^2\partial_\phi^2$ , it is written

$$(\overset{\circ}{\Delta} - \Omega^2\partial_\phi^2)h_{ab} = S_{ab} \quad (\text{A60})$$

with

$$\begin{aligned} S_{ab} &:= 2\bar{\mathcal{E}}_{ab}^{\text{TF}} - \frac{1}{3}\tilde{\gamma}_{ab}\overset{\circ}{D}^e h^{cd}\overset{\circ}{D}_e h_{cd} \\ &+ \frac{1}{3}\tilde{\gamma}_{ab}\Omega^2\partial_\phi h^{cd}\partial_\phi h_{cd}. \end{aligned} \quad (\text{A61})$$

Using the rescaled  $\tilde{A}_{ab}$ ,  $\bar{\mathcal{E}}_{ab}$  is defined by

$$\begin{aligned} \bar{\mathcal{E}}_{ab} &:= \tilde{R}_{ab}^{\text{D}} + \tilde{R}_{ab}^{\text{NL}} + {}^3\bar{R}_{ab}^\psi - \frac{1}{\alpha}\bar{D}_a\bar{D}_b\alpha + \frac{1}{3}\psi^4 K\tilde{A}_{ab} \\ & - 2\psi^4\tilde{A}_{ac}\tilde{A}_b{}^c + \frac{1}{\alpha}\mathfrak{L}_\omega(\psi^4\tilde{A}_{ab}) - \frac{1}{2}\Omega^2\partial_\phi^2 h_{ab} \\ & - 8\pi\bar{S}_{ab}, \end{aligned} \quad (\text{A62})$$

where a difference from (A59) is a term in the last line.

### e. Matter source terms

In the above, the matter source terms,  $\rho_H$ ,  $j_a$ ,  $S$  and  $S_{ab}$ , that appear in the field equations are obtained from the stress-energy tensor. We write the projection of the stress-energy tensor in terms of the fluid variables and metric potentials. The 4-velocity for irrotational flow  $u^\alpha = u^t(k^\alpha + v^\alpha)$  is decomposed with respect to the foliation  $\Sigma_t$  as

$$u^\alpha n_\alpha = -\alpha u^t \quad (\text{A63})$$

$$u^\alpha\gamma_{\alpha a} = u_a = \frac{1}{h}D_a\Phi = \frac{1}{h}\overset{\circ}{D}_a\Phi, \quad (\text{A64})$$

where the velocity potential  $\Phi$  is introduced by  $hu_\alpha = \nabla_\alpha\Phi$ .

Using these relations, the matter source terms of the field equations become

$$\rho_H := T_{\alpha\beta}n^\alpha n^\beta = h\rho(\alpha u^t)^2 - p, \quad (\text{A65})$$

$$j_a := -T_{\alpha\beta}\gamma_a{}^\alpha n^\beta = \rho\alpha u^t\overset{\circ}{D}_a\Phi, \quad (\text{A66})$$

$$S := T_{\alpha\beta}\gamma^{\alpha\beta} = h\rho[(\alpha u^t)^2 - 1] + 3p, \quad (\text{A67})$$

$$S_{ab} := T_{\alpha\beta}\gamma_a^\alpha\gamma_b^\beta = \frac{\rho}{h}\overset{\circ}{D}_a\Phi\overset{\circ}{D}_b\Phi + p\gamma_{ab}, \quad (\text{A68})$$

or with a barred quantity,

$$\bar{S}_{ab} = \frac{\rho}{h}\overset{\circ}{D}_a\Phi\overset{\circ}{D}_b\Phi. \quad (\text{A69})$$

### 3. Equations for irrotational fluid

Following Sec. II C and II D, a set of equations used in our codes to solve for the matter variables are derived. As independent variables, we choose the relativistic enthalpy per baryon mass, the time component of the 4-velocity, and the velocity potential,  $\{h, u^t, \Phi\}$ . For the first two variables, the first integral Eq. (34) and the normalization of the 4-velocity  $u_\alpha u^\alpha = -1$  are solved. Using a relation derived from Eqs. (31) and (32),

$$v_a + \omega_a = \frac{1}{hu^t}D_a\Phi, \quad (\text{A70})$$

these equations are rewritten,

$$h = \left[ \frac{1}{\alpha^2}(\mathcal{E} + \omega^a D_a\Phi)^2 - D_a\Phi D^a\Phi \right]^{1/2}, \quad (\text{A71})$$

$$u^t = \frac{1}{\alpha^2 h}(\mathcal{E} + \omega^a D_a\Phi), \quad (\text{A72})$$

where the first one is from  $u_\alpha u^\alpha = -1$ , and the second from Eq. (34).

An equation to calculate the velocity potential  $\Phi$  is derived from the rest-mass conservation law, Eq. (26),

$$\begin{aligned} \frac{1}{\sqrt{-g}}\mathcal{E}_u(\rho\sqrt{-g}) &= \frac{1}{\alpha\sqrt{\gamma}}\mathcal{E}_v(\rho u^t \alpha\sqrt{\gamma}) \\ &= \frac{1}{\alpha}D_a(\alpha\rho u^t v^a) = 0. \end{aligned} \quad (\text{A73})$$

Substituting Eq. (A70) in the above relation, we have an elliptic equation for  $\Phi$ ,

$$D^a D_a\Phi = D_a(hu^t\omega^a) - (D_a\Phi - hu^t\omega_a)\frac{h}{\alpha\rho}D^a\frac{\alpha\rho}{h}. \quad (\text{A74})$$

This equation is solved with Neumann boundary condition to impose the fluid 4-velocity  $u^\alpha$  to follow the surface of the star. The surface is defined by the vanishing pressure  $p = 0$ , which coincide with the  $h = 1$  surface in our EOS (see Sec II D). Hence, the boundary condition is written

$$u^\alpha\nabla_\alpha h = 0 \quad \text{at} \quad h = 1, \quad (\text{A75})$$

and, using  $\mathcal{E}_k h = 0$  and Eq. (A70), Neumann boundary condition for the potential  $\Phi$  is rewritten,

$$(D^a\Phi - hu^t\omega^a)D_a h = 0, \quad (\text{A76})$$

where  $D_a h$  is normal to the stellar surface.

Finally, we rewrite the above set of equations for the helically symmetric irrotational flow using the flat derivative  $\overset{\circ}{D}_a$ :

$$h = \left[ \frac{1}{\alpha^2}(\mathcal{E} + \tilde{\omega}^a \overset{\circ}{D}_a\Phi)^2 - \frac{1}{\psi^4}\tilde{\gamma}^{ab}\overset{\circ}{D}_a\Phi\overset{\circ}{D}_b\Phi \right]^{1/2}, \quad (\text{A77})$$

$$u^t = \frac{1}{\alpha^2 h}(\mathcal{E} + \tilde{\omega}^a \overset{\circ}{D}_a\Phi), \quad (\text{A78})$$

$$\overset{\circ}{\Delta}\Phi = \mathcal{S}, \quad (\text{A79})$$

where  $\mathcal{S}$  is defined by

$$\begin{aligned} \mathcal{S} &= -h^{ab}\overset{\circ}{D}_a\overset{\circ}{D}_b\Phi + \tilde{\gamma}^{ab}C_{ab}^c\overset{\circ}{D}_c\Phi - \frac{2}{\psi}\tilde{\gamma}^{ab}\overset{\circ}{D}_a\psi\overset{\circ}{D}_b\Phi \\ &\quad + \frac{1}{\psi^2}\tilde{\omega}^a\overset{\circ}{D}_a(hu^t\psi^6) + \psi^4 hu^t \overset{\circ}{D}_a\tilde{\omega}^a \\ &\quad - (\tilde{\gamma}^{ab}\overset{\circ}{D}_b\Phi - \psi^4 hu^t \tilde{\omega}^a)\frac{h}{\alpha\rho}\overset{\circ}{D}_a\frac{\alpha\rho}{h}, \end{aligned} \quad (\text{A80})$$

and, for  $\tilde{\gamma} = f$ ,  $\overset{\circ}{D}_a\tilde{\omega}^a = \overset{\circ}{D}_a\tilde{\omega}^a = \overset{\circ}{D}_a\tilde{\beta}^a$ .

## APPENDIX B: SELF-CONSISTENT FIELD ITERATION SCHEME

### 1. Elliptic equation solver

As mentioned in Sec. III B, components of the metric are computed on a spherical-coordinate grid whose origin is placed at the center of mass. The momentum constraints and the tracefree part of Einstein's equation are a spatial vector and a tensor equation, respectively, and it would be natural to write the equations in components along the spherical coordinates [36]. It is simpler, however, to solve these equations for Cartesian components, yet on the spherical coordinates, because each Cartesian component satisfies a field equation whose principal part is the same as that of a scalar equation.

For the spatial tracefree part of Einstein's equation solved for the nonconformally flat part  $h_{ab}$ , writing the principal part  $\mathcal{L} := \overset{\circ}{\Delta}$  or  $\overset{\circ}{\Delta} - \Omega^2\partial_\phi^2$ , the field equations become

$$\mathcal{L}h_{ab} = \mathcal{S}_{ab}. \quad (\text{B1})$$

Expanding each Cartesian component of  $h_{ab}$  in scalar multipoles, the equation with the operator  $\overset{\circ}{\Delta} - \Omega^2\partial_\phi^2$  becomes a Helmholtz equation for each mode,

$$(\overset{\circ}{\Delta} + m^2\Omega^2)h_{ab}^{\ell m}Y_{\ell m} = \mathcal{S}_{ab}^{\ell m}Y_{\ell m}. \quad (\text{B2})$$

Hence these elliptic equations are integrated using Green's formula,

$$\begin{aligned}
h_{ab}(x) = & -\frac{1}{4\pi} \int_V G(x, x') \mathcal{S}_{ab}(x') d^3x' \\
& + \frac{1}{4\pi} \int_{\partial V} [G(x, x') \overset{\circ}{D}'^c h_{ab}(x') \\
& - h_{ab}(x') \overset{\circ}{D}'^c G(x, x')] dS'_c, \quad (\text{B3})
\end{aligned}$$

where  $x$  and  $x'$  are positions,  $x, x' \in V \subseteq \Sigma_t$ , and the Green function  $G(x, x')$  satisfies

$$\mathcal{L} G(x, x') = -4\pi \delta(x - x'). \quad (\text{B4})$$

We choose the Green function  $G(x, x')$  without boundary for the BNS calculations.

For the Laplace operator,  $\mathcal{L} = \overset{\circ}{\Delta}$ , a multipole expansion of  $G(x, x')$  in associated Legendre functions on the spherical coordinate is written

$$\begin{aligned}
G(x, x') = & \frac{1}{|x - x'|} \\
= & \sum_{\ell=0}^{\infty} g_{\ell}(r, r') \sum_{m=0}^{\ell} \epsilon_m \frac{(\ell - m)!}{(\ell + m)!} P_{\ell}^m(\cos\theta) \\
& \times P_{\ell}^m(\cos\theta') \cos m(\varphi - \varphi'), \quad (\text{B5})
\end{aligned}$$

where the radial Green function  $g_{\ell}(r, r')$  becomes

$$g_{\ell}(r, r') = \frac{r_{<}^{\ell}}{r_{>}^{\ell+1}}, \quad (\text{B6})$$

with  $r_{>} := \max\{r, r'\}$ ,  $r_{<} := \min\{r, r'\}$ , and the coefficients  $\epsilon_m$  are equal to  $\epsilon_0 = 1$  for  $m = 0$ , and  $\epsilon_m = 2$  for  $m \geq 1$ .

For the case with the Helmholtz operator,  $\mathcal{L} = \overset{\circ}{\Delta} + m^2 \Omega^2$ , we choose the Green function for the half-retarded + half-advanced field [11],

$$\begin{aligned}
G(x, x') = & \sum_{\ell=0}^{\infty} \sum_{m=0}^{\ell} g_{\ell m}(r, r') \epsilon_m \frac{(\ell - m)!}{(\ell + m)!} P_{\ell}^m(\cos\theta) \\
& \times P_{\ell}^m(\cos\theta') \cos m(\varphi - \varphi'), \quad (\text{B7})
\end{aligned}$$

where the radial Green function  $g_{\ell m}(r, r')$  is constructed from the spherical Bessel functions of the first and second kinds  $j_{\ell}(x)$  and  $n_{\ell}(x)$ ,

$$g_{\ell m}(r, r') = \begin{cases} \frac{r_{<}^{\ell}}{r_{>}^{\ell+1}}, & \text{for } m = 0, \\ -m\Omega(2\ell + 1)j_{\ell}(m\Omega r_{<})n_{\ell}(m\Omega r_{>}), & \text{for } m \geq 1. \end{cases} \quad (\text{B8})$$

## 2. Summary for iteration scheme

Equation (B3) is used as an elliptic equation solver for the field variables  $\{\alpha, \beta_a, \psi, h_{ab}\}$ . In the code, the elliptic solver is used to compute the combination  $\alpha\psi$  from Eq. (A41); to compute the potentials (A32) of the shift vector  $\tilde{\beta}_a$  from Eqs. (A43) and (A35); and to compute the gauge potentials (49) from Eq. (50).

For the fluid variables,  $\{h, u^i, \Phi\}$  are found from Eqs. (A77)–(A79), respectively. A detailed description of a method to solve Eq. (A79) is found in [36]. As we use the surface-fitted coordinates to calculate neutron stars, the surface  $R(\theta_f, \phi_f)$  becomes an additional variable. A stellar surface is defined by the pressure  $p = 0$ , and, instead, it is located by a condition  $q = p/\rho = 0$  in the code.

A solution is specified by two parameters for an equal mass binary, which we take to be the orbital angular momentum and the injection energy,  $\{\Omega, \mathcal{E}\}$ . We introduce one more parameter  $R_0$  to normalize the radial coordinate, where  $R_0$  is half the coordinate diameter of a neutron star along the  $(\theta_f, \phi_f) = (\pi/2, 0)$  line. These parameters are calculated from the conditions  $R(\pi/2, 0)/R_0 = 1$  and  $R(\pi/2, \pi)/R_0 = 1$ , after prescribing a value of a thermodynamic variable at a point in a star, for which a central

value of  $h$  is fixed at  $r_f = 0$ . These conditions are applied to Eq. (A77), and solved for the three parameters.

All these variables are assigned on each grid point, and the parameters are calculated from the equations mentioned above in each iteration cycle. If we represent the set of fluid and metric variables by  $\hat{\Psi}$ , we can describe the iteration schematically as follows. The variables are updated from their values at the  $N$ th iteration cycle,  $\Psi^{(N)}$ , to the  $(N + 1)$ th,  $\Psi^{(N+1)}$ , using softening, in the manner

$$\Psi^{(N+1)} = \lambda \hat{\Psi} + (1 - \lambda) \Psi^{(N)}, \quad (\text{B9})$$

where  $\lambda$  is the softening parameter, chosen to be in the range 0.1 to 0.3 to accelerate convergence. For a criteria to determine convergence, a relative difference of successive cycles

$$\frac{2|\Psi^{(N+1)} - \Psi^{(N)}|}{|\Psi^{(N+1)}| + |\Psi^{(N)}|} < \delta \quad (\text{B10})$$

is used, with  $\delta = 10^{-6}$  in the present calculations.

### APPENDIX C: FORMULAS FOR MASS AND ANGULAR MOMENTUMS

Definitions of the quantities shown in tables and figures, which characterize a solution of BNS, and their expressions used in actual numerical computations, are summarized in this Appendix.

The rest mass is the baryon mass density measured by comoving observers integrated over the initial hypersurface, and during the inspiral phase of binary neutron star, it is considered to be conserved. The rest mass of one component of a binary system is written  $M_0$  and defined by

$$M_0 := \int_{\Sigma} \rho u^\alpha dS_\alpha = \int_{\Sigma} \rho u^t \alpha \psi^6 \sqrt{\tilde{\gamma}} d^3x, \quad (C1)$$

where  $dS_\alpha = \nabla_\alpha t \sqrt{-g} d^3x$ , and  $\sqrt{-g} d^3x = \alpha \psi^6 \sqrt{\tilde{\gamma}} d^3x = \alpha \psi^6 r^2 \sin\theta dr d\theta d\phi$ , because  $\tilde{\gamma} = f$  is assumed.

In this paper, the mass  $M_1$  is used to specify an equal mass BNS sequence, and  $M = 2M_1$  is used to normalize quantities.  $M_1$  is the gravitational mass of a single spherical star whose rest mass is equal to the rest mass  $M_0$  of one neutron star in the binary system of each model (see Table III).

The ADM mass  $M_{\text{ADM}}$  is rewritten using conformal spatial metric,

$$\begin{aligned} M_{\text{ADM}} &:= \frac{1}{16\pi} \int_{\infty} (f^{ac} f^{bd} - f^{ab} f^{cd}) \overset{\circ}{D}_b \gamma_{cd} dS_a \\ &= \frac{1}{16\pi} \int_{\infty} (f^{ac} f^{bd} - f^{ab} f^{cd}) \overset{\circ}{D}_b \tilde{\gamma}_{cd} dS_a \\ &\quad + \frac{1}{16\pi} \int_{\infty} (-2) f^{ab} \overset{\circ}{D}_b \psi^4 dS_a \\ &= -\frac{1}{2\pi} \int_{\infty} \overset{\circ}{D}_a \psi dS_a, \end{aligned} \quad (C2)$$

where, in the second equality, the first term vanishes because of our choice  $\tilde{\gamma} = f$ ; and  $\psi \rightarrow 1$  is used in the second term. We have calculated approximate values of  $M_{\text{ADM}}$  using this surface integral at the boundary of the computational domain. Also, we fit  $M_\psi/2r$  to  $\psi - 1$  near the boundary, to ensure a constant  $M_\psi \approx M_{\text{ADM}}$ . In the tables, however, the values of  $M_{\text{ADM}}$  are calculated from a formula in which the above surface integral is converted to a volume integral using the Gauss-Stokes lemma. We apply this on the conformal spatial hypersurface, which results in a simpler formula; since, at spatial infinity  $\psi \rightarrow 1$ ,  $\tilde{\gamma}^{ab} \rightarrow f^{ab}$  and  $dS_a = \nabla_a r \sqrt{f} d^2x = \nabla_a r \sqrt{\tilde{\gamma}} d^2x =: d\tilde{S}_a$ , we have

$$\begin{aligned} M_{\text{ADM}} &= -\frac{1}{2\pi} \int_{\infty} \overset{\circ}{D}^a \psi d\tilde{S}_a = -\frac{1}{2\pi} \int_{\Sigma} \tilde{\Delta} \psi d\tilde{S}, \\ &= \frac{1}{2\pi} \int_{\Sigma} \left[ -\frac{\psi}{8} {}^3\tilde{R} + \frac{1}{8} \psi^5 \left( \tilde{A}_{ab} \tilde{A}^{ab} - \frac{2}{3} K^2 \right) \right. \\ &\quad \left. + 2\pi \psi^5 \rho_H \right] \sqrt{\tilde{\gamma}} d^3x. \end{aligned} \quad (C3)$$

The Komar mass associated with a timelike Killing field  $t^\alpha$  is written

$$\begin{aligned} M_K &:= -\frac{1}{4\pi} \int_{\infty} \nabla^\alpha t^\beta dS_{\alpha\beta} = -\frac{1}{4\pi} \int_{\Sigma} R^\alpha{}_\beta t^\beta dS_\alpha \\ &= \int_{\Sigma} (2T^\alpha{}_\beta - T g^\alpha{}_\beta) t^\beta dS_\alpha, \\ &= \int_{\Sigma} [\alpha(\rho_H + S) - 2j_a \beta^a] \psi^6 \sqrt{\tilde{\gamma}} d^3x, \end{aligned} \quad (C4)$$

where  $dS_\alpha = n_\alpha \sqrt{\tilde{\gamma}} d^3x$  is used. To derive this, the global existence of a timelike Killing field is assumed. For the spacetime of WL/NHS formulations, no such timelike Killing field exists. Instead, an asymptotic Komar mass can be written

$$\begin{aligned} M_K &:= -\frac{1}{4\pi} \int_{\infty} \nabla^\alpha t^\beta dS_{\alpha\beta} = \frac{1}{4\pi} \int_{\infty} D^a \alpha dS_a \\ &= \frac{1}{4\pi} \int_{\Sigma} \Delta \alpha d\Sigma \\ &= \frac{1}{4\pi} \int_{\Sigma} \left[ \left( \alpha \tilde{A}_{ab} \tilde{A}^{ab} + \frac{1}{3} K^2 \right) \right. \\ &\quad \left. + \mathcal{L}_\omega K + 4\pi \alpha (\rho_H + S) \right] \psi^6 \sqrt{\tilde{\gamma}} d^3x, \end{aligned} \quad (C5)$$

where  $(G_{\alpha\beta} - 8\pi T_{\alpha\beta})g^{\alpha\beta} = 0$  is used.

In [10], we have derived asymptotic conditions for an equality of the ADM mass, and the asymptotic Komar mass [39],  $M_{\text{ADM}} = M_K$ . The equality is related to the relativistic virial relation for the equilibrium [40],

$$\int x^a \gamma_a{}^\alpha \nabla_\beta T_\alpha{}^\beta \sqrt{-g} d^3x = 0. \quad (C6)$$

In the WL/NHS formulation the asymptotic fall-off of each field is sufficiently fast to enforce the equality. And in this case, the above two definitions for  $M_K$  agree as well.

Finally, the total angular momentum is calculated from a volume form of surface integral at spatial infinity

$$J := -\frac{1}{8\pi} \int_{\infty} \pi^a{}_b \phi^b dS_a = \frac{1}{8\pi} \int_{\infty} K^a{}_b \phi^b dS_a. \quad (C7)$$

To calculate  $J$ , we set the surface near the boundary of the computational domain of the central coordinates and use the Gauss-Stokes lemma to write

$$\begin{aligned} J &= \frac{1}{8\pi} \int_{\Sigma} D_a (K^a{}_b \phi^b) dS \\ &= \frac{1}{8\pi} \int_{\Sigma} (8\pi j_a \phi^a + K^a{}_b D_a \phi^b) dS. \\ &= \frac{1}{8\pi} \int_{\Sigma} \left( 8\pi j_a \phi^a + A^a{}_b \overset{\circ}{D}_a \phi^b \right. \\ &\quad \left. + \frac{2}{\psi} K \phi^a \overset{\circ}{D}_a \psi \right) \psi^6 \sqrt{\tilde{\gamma}} d^3x. \end{aligned} \quad (C8)$$

The values of  $J$  listed in the tables in next section, are calculated from the latter formula.

### APPENDIX D: SELECTED SOLUTION SEQUENCES

Selected waveless solutions of irrotational BNS for parametrized EOS presented in Table III of Sec. IV are

TABLE IV. Solution sequence for the EOS 2H.

$d/R_0$	$2d/M$	$R_0/M$	$\Omega M$	$M_{\text{ADM}}$	$J/M^2$
1.3125	9.2784	7.0693	0.030 149	2.671 91	0.966 37
1.3438	9.4190	7.0095	0.029 649	2.672 06	0.968 19
1.3750	9.5654	6.9566	0.029 126	2.672 23	0.970 48
1.4375	9.8715	6.8671	0.028 019	2.672 65	0.975 82
1.5000	10.192	6.7948	0.026 901	2.673 11	0.982 79
1.6250	10.873	6.6912	0.024 693	2.674 22	0.999 05
1.7500	11.590	6.6229	0.022 648	2.675 37	1.0178
1.8750	12.330	6.5759	0.020 794	2.676 48	1.0375
2.0000	13.090	6.5451	0.019 118	2.677 56	1.0572
2.5000	16.234	6.4936	0.014 113	2.681 30	1.1415
3.0000	19.455	6.4852	0.010 889	2.684 04	1.2229

TABLE V. Solution sequence for the EOS HB.

$d/R_0$	$2d/M$	$R_0/M$	$\Omega M$	$M_{\text{ADM}}$	$J/M^2$
1.3750	6.8380	4.9731	0.045 877	2.665 07	0.890 82
1.4062	6.9403	4.9353	0.045 086	2.665 21	0.892 16
1.4375	7.0511	4.9051	0.044 231	2.665 36	0.893 78
1.5000	7.2800	4.8533	0.042 526	2.665 80	0.898 12
1.6250	7.7600	4.7754	0.039 177	2.666 88	0.908 29
1.7500	8.2681	4.7246	0.036 025	2.668 10	0.920 72
1.8750	8.7975	4.6920	0.033 145	2.669 32	0.934 85
2.0000	9.3425	4.6712	0.030 526	2.670 57	0.949 26
2.5000	11.606	4.6423	0.022 621	2.675 11	1.0132
3.0000	13.931	4.6435	0.017 521	2.678 60	1.0789

TABLE VI. Solution sequence for the EOS 2B.

$d/R_0$	$2d/M$	$R_0/M$	$\Omega M$	$M_{\text{ADM}}$	$J/M^2$
1.4375	5.5971	3.8936	0.059 912	2.661 09	0.856 42
1.4688	5.6801	3.8673	0.058 871	2.661 18	0.857 33
1.5000	5.7713	3.8475	0.057 759	2.661 33	0.858 40
1.5313	5.8622	3.8284	0.056 652	2.661 50	0.859 59
1.5625	5.9542	3.8107	0.055 575	2.661 71	0.860 99
1.6250	6.1443	3.7811	0.053 414	2.662 11	0.864 24
1.7500	6.5438	3.7393	0.049 241	2.663 18	0.872 25
1.8750	6.9613	3.7127	0.045 416	2.664 32	0.882 46
2.0000	7.3930	3.6965	0.041 907	2.665 55	0.893 11
2.5000	9.1954	3.6782	0.031 170	2.670 36	0.942 83
3.0000	11.050	3.6835	0.024 219	2.674 33	0.997 55

tabulated in Tables IV, V, VI, VII, VIII, IX, X, and XI. All quantities are dimensionless in the geometric units  $G = c = 1$ , except for the ADM mass which is in a unit of solar mass  $M_{\text{ADM}} [M_\odot]$ .

TABLE VII. Solution sequence for the EOS SLy.

$d/R_0$	$2d/M$	$R_0/M$	$\Omega M$	$M_{\text{ADM}}$	$J/M^2$
1.3750	6.7360	4.8989	0.046 804	2.664 79	0.8804
1.4375	6.9455	4.8316	0.045 130	2.665 05	0.8987
1.4687	7.0572	4.8049	0.044 256	2.665 26	0.8983
1.5000	7.1692	4.7795	0.043 403	2.665 46	0.8998
1.5625	7.4012	4.7367	0.041 683	2.666 00	0.8952
1.6250	7.6424	4.7030	0.039 990	2.666 55	0.9093
1.7500	8.1425	4.6529	0.036 778	2.667 77	0.9109
1.8750	8.6640	4.6208	0.033 842	2.668 99	0.9397
2.0000	9.2007	4.6004	0.031 172	2.670 25	0.9413
2.5000	11.431	4.5722	0.023 105	2.674 81	1.082
3.0000	13.721	4.5737	0.017 898	2.678 34	1.031

TABLE VIII. Solution sequence for the EOS APR1.

$d/R_0$	$2d/M$	$R_0/M$	$\Omega M$	$M_{\text{ADM}}$	$J/M^2$
1.6875	5.8207	3.4493	0.057 394	2.661 44	0.855 85
1.7500	6.0069	3.4325	0.055 113	2.661 95	0.859 33
1.8125	6.1950	3.4179	0.052 972	2.662 47	0.863 39
1.8750	6.3877	3.4068	0.050 902	2.663 02	0.867 70
1.9375	6.5845	3.3985	0.048 909	2.663 63	0.872 33
2.0000	6.7839	3.3920	0.047 008	2.664 23	0.877 06
2.5000	8.4399	3.3760	0.035 057	2.669 00	0.921 98
3.0000	10.148	3.3826	0.027 269	2.673 08	0.972 31

TABLE IX. Solution sequence for the EOS FPS.

$d/R_0$	$2d/M$	$R_0/M$	$\Omega M$	$M_{\text{ADM}}$	$J/M^2$
1.4375	6.3451	4.4140	0.050 851	2.663 31	0.874 58
1.4688	6.4477	4.3899	0.049 882	2.663 46	0.876 09
1.5000	6.5504	4.3669	0.048 919	2.663 64	0.877 82
1.5313	6.6534	4.3451	0.047 977	2.663 87	0.879 55
1.5625	6.7597	4.3262	0.047 029	2.664 15	0.881 56
1.6250	6.9799	4.2953	0.045 139	2.664 67	0.886 18
1.7500	7.4359	4.2491	0.041 551	2.665 85	0.896 72
1.8750	7.9127	4.2201	0.038 262	2.667 09	0.909 18
2.0000	8.4036	4.2018	0.035 261	2.668 35	0.921 83
2.5000	10.447	4.1786	0.026 166	2.673 04	0.979 44
3.0000	12.547	4.1822	0.020 291	2.676 77	1.0401

TABLE X. Solution sequence for the EOS BGN1H1.

$d/R_0$	$2d/M$	$R_0/M$	$\Omega M$	$M_{\text{ADM}}$	$J/M^2$
1.4062	7.7372	5.5020	0.038 958	2.667 49	0.914 13
1.4375	7.8579	5.4664	0.038 232	2.667 65	0.916 10
1.4688	7.9817	5.4344	0.037 499	2.667 86	0.918 47
1.5000	8.1086	5.4058	0.036 772	2.668 10	0.921 30
1.5625	8.3727	5.3585	0.035 291	2.668 67	0.927 11
1.6875	8.9226	5.2875	0.032 465	2.669 83	0.940 95
1.7500	9.2099	5.2628	0.031 101	2.670 46	0.948 04
1.8750	9.7970	5.2250	0.028 611	2.671 66	0.964 21
2.0000	10.402	5.2008	0.026 341	2.672 86	0.980 37
2.5000	12.914	5.1657	0.019 492	2.677 18	1.0507
3.0000	15.493	5.1643	0.015 068	2.680 40	1.1206

TABLE XI. Solution sequence for the EOS ALF3.

$d/R_0$	$2d/M$	$R_0/M$	$\Omega M$	$M_{\text{ADM}}$	$J/M^2$
1.4375	6.0667	4.2203	0.053 901	2.662 64	0.866 55
1.4688	6.1649	4.1974	0.052 878	2.662 79	0.867 85
1.5000	6.2628	4.1752	0.051 867	2.662 97	0.869 44
1.6250	6.6732	4.1066	0.047 891	2.663 96	0.877 18
1.6875	6.8881	4.0818	0.045 973	2.664 51	0.882 02
1.7500	7.1090	4.0623	0.044 109	2.665 12	0.887 09
1.8125	7.3353	4.0470	0.042 335	2.665 76	0.892 98
1.8750	7.5659	4.0352	0.040 622	2.666 35	0.898 78
2.0000	8.0365	4.0183	0.037 449	2.667 65	0.910 94
2.5000	9.9949	3.9980	0.027 806	2.672 37	0.966 16
3.0000	12.009	4.0031	0.021 559	2.676 20	1.0244

- [1] M. Miller, Phys. Rev. D **69**, 124013 (2004); M. Miller, P. Gressman, and W.-M. Suen, Phys. Rev. D **69**, 064026 (2004); M. Miller, Phys. Rev. D **71**, 104016 (2005).
- [2] J. R. Wilson and G. J. Mathews, Phys. Rev. Lett. **75**, 4161 (1995); P. Marronetti, G. J. Mathews, and J. R. Wilson, Phys. Rev. D **60**, 087301 (1999); T. W. Baumgarte, G. B. Cook, M. A. Scheel, S. L. Shapiro, and S. A. Teukolsky, Phys. Rev. D **57**, 6181 (1998); **57**, 7299 (1998); S. Bonazzola, E. Gourgoulhon, and J.-A. Marck, Phys. Rev. Lett. **82**, 892 (1999); E. Gourgoulhon, P. Grandclement, K. Taniguchi, J. A. Marck, and S. Bonazzola, Phys. Rev. D **63**, 064029 (2001); K. Taniguchi and E. Gourgoulhon, Phys. Rev. D **66**, 104019 (2002); **68**, 124025 (2003); J. A. Faber, P. Grandclement, F. A. Rasio, and K. Taniguchi, Phys. Rev. Lett. **89**, 231102 (2002); M. Bejger, D. Gondek-Rosinska, E. Gourgoulhon, P. Haensel, K. Taniguchi, and J. L. Zdunik, Astron. Astrophys. **431**, 297 (2005).
- [3] K. Uryu and Y. Eriguchi, Phys. Rev. D **61**, 124023 (2000); K. Uryu, M. Shibata, and Y. Eriguchi, Phys. Rev. D **62**, 104015 (2000).
- [4] F. Usui, K. Uryū, and Y. Eriguchi, Phys. Rev. D **61**, 024039 (1999).
- [5] K. Taniguchi, T. W. Baumgarte, J. A. Faber, and S. L. Shapiro, Phys. Rev. D **72**, 044008 (2005); **74**, 041502(R) (2006); **75**, 084005 (2007); **77**, 044003 (2008); K. Kyutoku, M. Shibata, and K. Taniguchi, Phys. Rev. D **79**, 124018 (2009); F. Foucart, L. E. Kidder, H. P. Pfeiffer, and S. A. Teukolsky, Phys. Rev. D **77**, 124051 (2008).
- [6] H. P. Pfeiffer, D. A. Brown, L. E. Kidder, L. Lindblom, G. Lovelace, and M. A. Scheel, Classical Quantum Gravity **24**, S59 (2007); J. G. Baker, S. T. McWilliams, J. R. van Meter, J. Centrella, D. -I. Choi, B. J. Kelly, and M. Koppitz, Phys. Rev. D **75**, 124024 (2007); M. Boyle, D. A. Brown, L. E. Kidder, A. H. Mroué, H. P. Pfeiffer, M. A. Scheel, G. B. Cook, and S. A. Teukolsky, Phys. Rev. D **76**, 124038 (2007); M. Hannam, S. Husa, J. A. González, U. Sperhake, and B. Brügmann, Phys. Rev. D **77**, 044020 (2008); M. Boyle, A. Buonanno, L. E. Kidder, A. H. Mroué, Y. Pan, H. P. Pfeiffer, and M. A. Scheel, Phys. Rev. D **78**, 104020 (2008).
- [7] K. Uryu, F. Limousin, J. L. Friedman, E. Gourgoulhon, and M. Shibata, Phys. Rev. Lett. **97**, 171101 (2006).
- [8] G. Schäfer and A. Gopakumar, Phys. Rev. D **69**, 021501(R) (2004).
- [9] S. Bonazzola, E. Gourgoulhon, P. Grandclement, and J. Novak, Phys. Rev. D **70**, 104007 (2004).
- [10] M. Shibata, K. Uryu, and J. L. Friedman, Phys. Rev. D **70**, 044044 (2004); **70**, 129901(E) (2004).
- [11] S. Yoshida, B. C. Bromley, J. S. Read, K. Uryu, and J. L. Friedman, Classical Quantum Gravity **23**, S599 (2006).
- [12] A report by J. Isenberg, “*Waveless Approximation Theories of Gravity*,” University of Maryland, 1978 has been published recently: J. Isenberg, Int. J. Mod. Phys. D **17**, 265 (2008); J. Isenberg and J. Nester, in *General Relativity and Gravitation*, edited by A. Held (Plenum Press, New York 1980), Vol. 1.
- [13] J. R. Wilson and G. J. Mathews, in *Frontiers in Numerical Relativity*, edited by C. R. Evans, L. S. Finn, and D. W. Hobill (Cambridge University Press, Cambridge, England, 1989), p. 306.
- [14] M. Shibata and K. Uryū, Phys. Rev. D **61**, 064001 (2000); Prog. Theor. Phys. **107**, 265 (2002); M. Shibata, K. Taniguchi, and K. Uryū, Phys. Rev. D **68**, 084020 (2003); **71**, 084021 (2005); M. Shibata and K. Taniguchi, Phys. Rev. D **73**, 064027 (2006); T. Yamamoto, M. Shibata, and K. Taniguchi, Phys. Rev. D **78**, 064054 (2008); K. Kiuchi, Y. Sekiguchi, M. Shibata, and K. Taniguchi, Phys. Rev. D **80**, 064037 (2009); M. D. Duez, P. Marronetti, S. L. Shapiro, and T. W. Baumgarte, Phys. Rev. D **67**, 024004 (2003); M. Anderson, E. W. Hirschmann, L. Lehner, S. L. Liebling, P. M. Motl, D. Neilsen, C. Palenzuela, and J. E. Tohline, Phys. Rev. D **77**, 024006 (2008); L. Baiotti, B. Giacomazzo, and L. Rezzolla, Phys. Rev. D **78**, 084033 (2008); R. Oechslin, K. Uryu, G. S. Poghosyan, and F. K. Thielemann, Mon. Not. R. Astron. Soc. **349**, 1469 (2004); R. Oechslin, H. T. Janka, and A. Marek, Astron. Astrophys. **467**, 395 (2007); R. Oechslin and H. T. Janka, Phys. Rev. Lett. **99**, 121102 (2007).
- [15] J. S. Read, C. Markakis, M. Shibata, K. Uryu, J. D. E. Creighton, and J. L. Friedman, Phys. Rev. D **79**, 124033 (2009).
- [16] Y. T. Liu, S. L. Shapiro, Z. B. Etienne, and K. Taniguchi, Phys. Rev. D **78**, 024012 (2008); M. Anderson, E. W. Hirschmann, L. Lehner, S. L. Liebling, P. M. Motl, D. Neilsen, C. Palenzuela, and J. E. Tohline, Phys. Rev.

- Lett. **100**, 191101 (2008); B. Giacomazzo, L. Rezzolla, and L. Baiotti, arXiv:0901.2722.
- [17] M. Shibata and K. Taniguchi, Phys. Rev. D **73**, 064027 (2006); M. Shibata and K. Uryū, Phys. Rev. D **74**, 121503(R) (2006); Classical Quantum Gravity **24**, S125 (2007); M. Shibata and K. Taniguchi, Phys. Rev. D **77**, 084015 (2008); M. Shibata, K. Kyutoku, T. Yamamoto, and K. Taniguchi, Phys. Rev. D **79**, 044030 (2009); Z. B. Etienne, J. A. Faber, Y. T. Liu, S. L. Shapiro, K. Taniguchi, and T. W. Baumgarte, Phys. Rev. D **77**, 084002 (2008); M. D. Duez, F. Foucart, L. E. Kidder, H. P. Pfeiffer, M. A. Scheel, and S. A. Teukolsky, Phys. Rev. D **78**, 104015 (2008); Z. B. Etienne, Y. T. Liu, S. L. Shapiro, and T. W. Baumgarte, Phys. Rev. D **79**, 044024 (2009).
- [18] J. S. Read, B. D. Lackey, B. J. Owen, and J. L. Friedman, Phys. Rev. D **79**, 124032 (2009).
- [19] J. K. Blackburn and S. Detweiler, Phys. Rev. D **46**, 2318 (1992); S. Detweiler, Phys. Rev. D **50**, 4929 (1994).
- [20] S. Bonazzola, E.ourgoulhon, and J.-A. Marck, Phys. Rev. D **56**, 7740 (1997).
- [21] J. L. Friedman, K. Uryu, and M. Shibata, Phys. Rev. D **65**, 064035 (2002); **70**, 129904(E) (2004).
- [22] E.ourgoulhon, P. Grandclément, and S. Bonazzola, Phys. Rev. D **65**, 044020 (2002); P. Grandclément, E.ourgoulhon, and S. Bonazzola, Phys. Rev. D **65**, 044021 (2002).
- [23] C. Klein, Phys. Rev. D **70**, 124026 (2004).
- [24] C. G. Torre, J. Math. Phys. (N.Y.) **44**, 6223 (2003); **47**, 073501 (2006).
- [25] J. P. Bruneton, AIP Conf. Proc. **861**, 558 (2006).
- [26] R. Beig, J. M. Heinzle, and B. G. Schmidt, Phys. Rev. Lett. **98**, 121102 (2007); J. Bica and B. G. Schmidt, Phys. Rev. D **76**, 104040 (2007).
- [27] J. T. Whelan, C. Beetle, W. Landry, and R. H. Price, Classical Quantum Gravity **19**, 1285 (2002); Z. Andrade *et al.*, Phys. Rev. D **70**, 064001 (2004); S. R. Lau and R. H. Price, J. Comput. Phys. **227**, 1126 (2007); C. Beetle, B. Bromley, N. Hernandez, and R. H. Price, Phys. Rev. D **76**, 084016 (2007); N. Hernandez and R. H. Price, Phys. Rev. D **79**, 064008 (2009).
- [28] J. L. Friedman and K. Uryu, Phys. Rev. D **73**, 104039 (2006); M. M. Glenz and K. Uryu, Phys. Rev. D **76**, 027501 (2007).
- [29] A. Schild, Phys. Rev. **131**, 2762 (1963).
- [30] C. S. Kochanek, Astrophys. J. **398**, 234 (1992); L. Bildsten and C. Cutler, Astrophys. J. **400**, 175 (1992).
- [31] K. Uryu and Y. Eriguchi, Mon. Not. R. Astron. Soc. **296**, L1 (1998); **299**, 575 (1998); K. Uryu and Y. Eriguchi, Astrophys. J. Suppl. Ser. **118**, 563 (1998); Y. Eriguchi and K. Uryu, Prog. Theor. Phys. Suppl. **136**, 199 (1999); K. Uryu and Y. Eriguchi, Mon. Not. R. Astron. Soc. **303**, 329 (1999); K. Taniguchi, Prog. Theor. Phys. **101**, 283 (1999); K. Taniguchi and T. Nakamura, Phys. Rev. Lett. **84**, 581 (2000); Phys. Rev. D **62**, 044040 (2000); K. Taniguchi, E.ourgoulhon, and S. Bonazzola, Phys. Rev. D **64**, 064012 (2001); K. Taniguchi and E.ourgoulhon, Phys. Rev. D **65**, 044027 (2002).
- [32] H. Asada, Phys. Rev. D **57**, 7292 (1998); M. Shibata, Phys. Rev. D **58**, 024012 (1998); S. A. Teukolsky, Astrophys. J. **504**, 442 (1998).
- [33] X. Huang, C. Markakis, N. Sugiyama, and K. Uryu, Phys. Rev. D **78**, 124023 (2008).
- [34] J. P. Ostriker and J. W.-K. Mark, Astrophys. J. **151**, 1075 (1968); I. Hachisu, Astrophys. J. Suppl. Ser. **62**, 461 (1986); **61**, 479 (1986); H. Komatsu, Y. Eriguchi, and I. Hachisu, Mon. Not. R. Astron. Soc. **237**, 355 (1989).
- [35] R. H. Price, C. Markakis, and J. L. Friedman, arXiv:0903.3074.
- [36] K. Uryū and Y. Eriguchi, Phys. Rev. D **61**, 124023 (2000); K. Uryū, M. Shibata, and Y. Eriguchi, Phys. Rev. D **62**, 104015 (2000).
- [37] A. A. Tsokaros and K. Uryu, Phys. Rev. D **75**, 044026 (2007).
- [38] H. Asada, M. Shibata, and T. Futamase, Prog. Theor. Phys. **96**, 81 (1996).
- [39] A. Komar, Phys. Rev. **113**, 934 (1959); **127**, 1411 (1962).
- [40] For the equality of  $M_{\text{ADM}} - M_{\text{K}}$ , see R. Beig, Phys. Lett. **69A**, 153 (1978); A. Ashtekar and A. Magnon-Ashtekar, J. Math. Phys. (N.Y.) **20**, 7931 (1979). For relativistic virial relations, see also, E.ourgoulhon and S. Bonazzola, Classical Quantum Gravity **11**, 443 (1994).
- [41] F. Douchin and P. Haensel, Astron. Astrophys. **380**, 151 (2001).
- [42] A. Akmal, V. R. Pandharipande, and D. G. Ravenhall, Phys. Rev. C **58**, 1804 (1998).
- [43] B. Friedman and V. R. Pandharipande, Nucl. Phys. **A361**, 502 (1981).
- [44] S. Balberg and A. Gal, Nucl. Phys. **A625**, 435 (1997).
- [45] M. Alford, M. Braby, M. Paris, and S. Reddy, Astrophys. J. **629**, 969 (2005).
- [46] L. Blanchet, Living Rev. Relativity **9**, 4 (2006), <http://www.livingreviews.org/lrr-2006-4>.
- [47] A. Buonanno, G. B. Cook, and F. Pretorius, Phys. Rev. D **75**, 124018 (2007); M. Boyle, D. A. Brown, L. E. Kidder, A. H. Mroue, H. P. Pfeiffer, M. A. Scheel, G. B. Cook, and S. A. Teukolsky, Phys. Rev. D **76**, 124038 (2007).
- [48] E. E. Flanagan and T. Hinderer, Phys. Rev. D **77**, 021502 (R) (2008); T. Hinderer, Astrophys. J. **677**, 1216 (2008); E. Berti, S. Iyer, and C. M. Will, Phys. Rev. D **77**, 024019 (2008); T. Damour and A. Nagar, arXiv:0906.0096 [Phys. Rev. D (to be published)]; T. Binington and E. Poisson, arXiv:0906.1366 [Phys. Rev. D (to be published)].
- [49] J. S. Read (private communication).
- [50] L. M. Lin and J. Novak, Classical Quantum Gravity **23**, 4545 (2006).
- [51] K. Kiuchi and S. Yoshida, Phys. Rev. D **78**, 044045 (2008); K. Kiuchi, K. Kotake, and S. Yoshida, arXiv:0904.2044.